European Journal of Medicinal Chemistry 228 (2022) 113971

Contents lists available at ScienceDirect

European Journal of Medicinal Chemistry

journal homepage: http://www.elsevier.com/locate/ejmech

Antitumor activity of novel POLA1-HDAC11 dual inhibitors

Sabrina Dallavalle [a, *], Loana Musso [a], Raffaella Cincinelli [a], Nadine Darwiche [b], Silvia Gervasoni [c], Giulio Vistoli [c], Mario B. Guglielmi [d], Ilaria La Porta [d], Maddalena Pizzulo [d], Elisa Modica [d], Federica Prosperi [d], Giacomo Signorino [d], Fabiana Colelli [d], Francesco Cardile [d], Alessandra Fucci [d], Egildo Luca D'Andrea [d], Assunta Riccio [d], Claudio Pisano [d, **]

[a] Department of Food, Environmental and Nutritional Sciences, Università degli Studi di Milano, via Celoria 2, 20133 Milano, Italy
[b] Department of Biochemistry and Molecular Genetics, Faculty of Medicine, American University of Beirut, Beirut, Lebanon
[c] Department of Pharmaceutical Sciences, Università degli Studi di Milano, via Mangiagalli 25, Milano, 20133, Italy
[d] Biogem, Institute of Molecular Biology and Genetics, Via Camporeale, 83031 Ariano Irpino(AV), Italy

A R T I C L E I N F O

Article history:
Received 14 June 2021
Received in revised form
29 October 2021
Accepted 31 October 2021
Available online 3 November 2021

Keywords:
DNA polymerase α
Histone deacetylases
HDAC11
Interferon-α
p53 acetylation

A B S T R A C T

Hybrid molecules targeting simultaneously DNA polymerase α (POLA1) and histone deacetylases (HDACs) were designed and synthesized to exploit a potential synergy of action. Among a library of screened molecules, MIR002 and GEM144 showed antiproliferative activity at nanomolar concentrations on a panel of human solid and haematological cancer cell lines. *In vitro* functional assays confirmed that these molecules inhibited POLA1 primer extension activity, as well as HDAC11. Molecular docking studies also supported these findings. Mechanistically, MIR002 and GEM144 induced acetylation of p53, activation of p21, G1/S cell cycle arrest, and apoptosis. Oral administration of these inhibitors confirmed their antitumor activity in *in vivo* models. In human non-small cancer cell (H460) xenografted in nude mice MIR002 at 50 mg/kg, Bid (qd × 5 × 3w) inhibited tumor growth (TGI = 61%). More interestingly, in POLA1 inhibitor resistant cells (H460-R9A), the *in vivo* combination of MIR002 with cisplatin showed an additive antitumor effect with complete disappearance of tumor masses in two animals at the end of the treatment. Moreover, in two human orthotopic malignant pleural mesothelioma xenografts (MM473 and MM487), oral treatments with MIR002 and GEM144 confirmed their significant antitumor activity (TGI = 72−77%).

Consistently with recent results that have shown an inverse correlation between POLA1 expression and type I interferon levels, MIR002 significantly upregulated interferon-α in immunocompetent mice.

1. Introduction

A well-established strategy in tumour treatment is the rational design of drug combinations. However, this approach has a number of limitations, mainly due to incompatible pharmacokinetics, multiple drug-drug interactions and loss of therapeutic flexibility [1]. An emerging alternative strategy is the development of hybrid bifunctional agents designed to simultaneously inhibit multiple cellular targets relevant to tumour growth/survival [2,3]. The interest towards multitarget ligands is becoming a paradigm in drug discovery for its potential benefits, including the modulation of drug resistance [4].

DNA polymerase α (POLA1), encoded by gene *POLA1*, is an enzyme that initiates DNA synthesis by using a RNA primer to synthesize the first ~10−20 base pairs of DNA, thereby providing the substrate for more processive DNA polymerases [5]. POLA1 is an ideal enzymatic target for drugs that block DNA replication, since it acts at the initial stage of DNA synthesis and is involved in the control of cell growth [6,7]. Interest in this target recently increased due to the finding that POLA1 regulates the activation of type I interferons, involved in the immune response [6]. With the development of tumor immunotherapy, immune regulation activities of small molecules and biological agents have become a hot research area [8]. Surprisingly, despite the evident clinical utility of

* Corresponding author.
** Corresponding author.
E-mail addresses: sabrina.dallavalle@unimi.it (S. Dallavalle), claudio.pisano@biogem.it (C. Pisano).

https://doi.org/10.1016/j.ejmech.2021.113971

anticancer therapies targeting essential components of DNA replication and modulating the immune response, there are no currently available drugs that directly inhibit POLA1. A recent paper reported that the compound CD437 (Fig. 1) acts as a potent POLA1 inhibitor [9]. CD437 belongs to the class of Retinoid Related Molecules (RRMs) [10], whose antitumor activity is independent from the activation of the retinoid nuclear receptors (RARs and RXRs) [11–13]. The finding that CD437 is able to inhibit POLA1, together with evidence that RRMs are not associated with cross-resistance mechanisms [9], opens a new investigation path. In the past few years, we have synthesized and studied several RRMs [14]. Interestingly, we have recently found that one of these compounds, ST1926 (Adarotene) [15–17] and some analogues (Fig. 1), also show potent POLA1 inhibition [18,19].

Another promising target in cancer therapy is represented by histone deacetylases (HDACs) [20–22]. The levels of histone acetylation play a crucial role in chromatin remodeling and in the regulation of gene transcription and aberrant histone modifications are frequently observed during tumorigenesis [20]. HDAC inhibition results in tumor differentiation and cell growth arrest. Most HDAC inhibitors contain a zinc-binding group (ZBG), frequently a hydroxamic acid, connected by a linker to a group, called cap, required for the recognition of the specific HDAC subclass [21,22] (Fig. 1). Four HDAC inhibitors are currently in clinical practice [21,22].

It is important to note that HDAC inhibitors are endowed with immune-enhancing effects [23] and potentiate the immune response by activating type I interferon, as well as POLA1 inhibitors.

The aim of our research has been to obtain hybrid molecules simultaneously targeting POLA1, involved in the early stage of DNA replication, and HDACs, acting on the modulation of genes expression essential for tumor growth.

To this scope, we designed a small library of potential dual-acting molecules containing the ST1926 scaffold, which should work as POLA1 inhibitor, connected by an appropriate linker to a ZBG, in order to achieve an effective HDAC inhibition. The hydroxamic acid moiety was selected as ZBG, due to its potent zinc binding ability, as testified by its presence in most of the HDAC inhibitors under clinical investigation.

Previous works showed that the metabolic instability of ST1926 and analogues is mainly due to the presence of the phenolic hydroxyl group, easily prone to glucuronidation [24]. For this reason, we attached the hydroxamic acid ZBG to the phenolic OH by a carbon chain with increasing length (compounds **1a**, **1d-g**, Fig. 1). We conceived that the introduction of this group would not vastly perturb the ability of the resulting compounds to inhibit HDAC, as the biphenyl core could work as a cap group. To enable a more thorough exploration of HDAC inhibitory activity, a structurally related analogue of compound **1a** was obtained replacing the zinc-binding hydroxamic acid with a carboxylic acid group (**2a**).

Herein we report the results of our efforts, which led to the identification of first-in-class POLA1-HDAC11 inhibitors as anticancer agents endowed with a novel pharmacological profile.

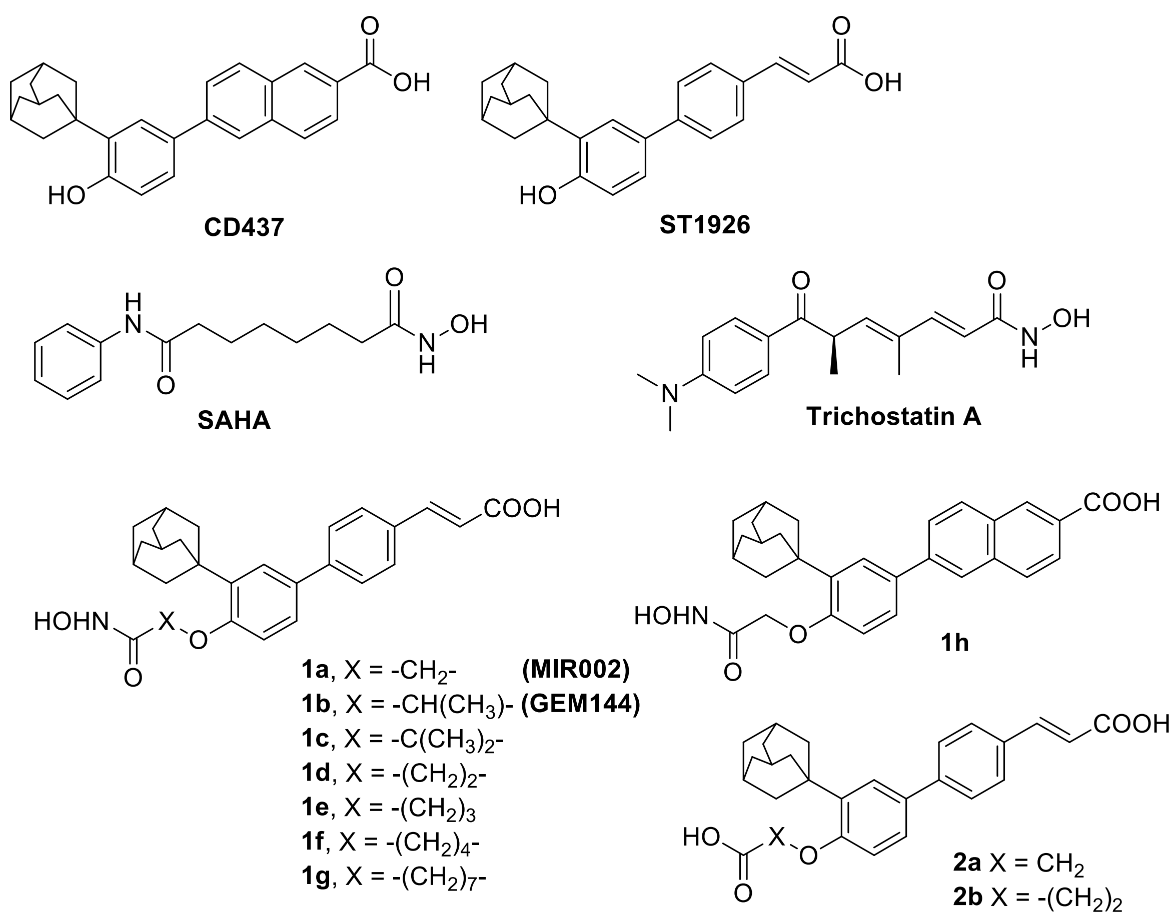

Fig. 1. Structures of representative RRM, HDAC inhibitors and the new compounds **1a-h** and **2a-b**.

2. Results and discussion

2.1. Chemistry

The compounds were prepared by a general procedure based on the alkylation of the *t*-butyl ester of ST1926 with suitable ethyl bromoalkylcarboxylates, followed by hydrolysis of the ethyl ester groups by LiOH, and coupling with NH_2OTHP to give the tetrahydropyranyl protected hydroxamic acids. Treatment with TFA removed both the THP protecting group and the t-butylester to afford the final compounds (Scheme 1). The α-methyl and α,α-dimethyl analogues of compound **1a** (compounds **1b** and **1c**, respectively) and the corresponding acid of **1d** (compound **2b**) were prepared as well. Finally, for a comparative evaluation, an analogue of CD437 (**1h**) containing the same features of compound **1a** was prepared following a similar synthetic procedure (Scheme 1).

2.2. Antiproliferative activity evaluation

The compounds were screened against an array of human cancer cell lines belonging to different tumor types. Since the new molecules were assumed to exert two distinct inhibitory functions on both POLA1 and HDACs, their activities were compared to that of ST1926/CD437, as specific POLA1 inhibitors, and SAHA, as a pan-HDAC inhibitor.

First, the compounds were screened on parental H460-non-small cell lung cancer (NSCLC) cells. In parallel, they were tested on a H460-R9A clone, 70-fold more resistant to ST1926 with respect to the parental NCI−H460 cell line [25], to select for compounds with a lower grade of resistance with respect to the previous cited molecule (Table 1). Most of the new retinoid derivatives showed a significant increase of cytotoxic activity against H460-R9A compared to ST1926. Compound **1a** (MIR002), with a short two-carbon chain linked to the phenolic oxygen, was identified as one of the most active ones, while compounds with longer chains showed a lower cytotoxicity. The introduction of a methyl group in position alpha to the hydroxamic acid moiety gave an equipotent compound (compound **1b**, GEM144), whereas a second methyl group (**1c**) slightly decreased the activity. The analogues of **1a** and **1d** containing a carboxylic acid moiety in place of the hydroxamic acid (**2a-b**) showed $IC_{50} > 10$ μM, highlighting the role of the zinc binding group in the activity of these compounds.

Noteworthy, MIR002 and GEM144 showed lower IC_{50} against H460-R9A cells with respect to ST1926 and CD437, with a consequent reduction of the IC_{50} ratio (RI) between resistant and parental cells (MIR002 and GEM144: R.I. = 11.2 and 8.5, respectively; ST1926 and CD437: R.I. = 70 and 56, respectively). These results highlight how the introduction of the hydroxamic acid moiety enhanced the pharmacological response of cells resistant to CD437 and ST1926.

To investigate whether these new molecules could be putatively administered *via* oral route, the cytotoxicity was evaluated in the A2780 ovarian cancer cell line and its multidrug resistant derivative A2780-DX, overexpressing P-glycoprotein (PgP), which is mainly responsible for the xenobiotic efflux and reduced intestinal drug absorption (Table 1). All the tested compounds retained their cytotoxic effects in A2780-DX, thus indicating that they are not PgP substrates and therefore putatively suitable for oral administration in patients. Based on these results, MIR002 and GEM144 were selected for further investigation. The wide spectrum of antiproliferative activity was confirmed by their evaluation against a wider panel of human cancer cell lines, including three malignant mesothelioma cell lines (MM432, MM473, MM487), six hematological tumor cell lines, human breast cancer (MDA-MB231 and MDA-MB436) and human glioma (U87MG) cell lines. (Table 2). Overall, the results of our preliminary screening uncover compounds MIR002 and GEM144 as the most promising molecules of the series.

2.3. POLA1 and HDAC11 inhibition

In order to understand the molecular mechanisms mediating the antitumor effects of MIR002 and GEM144, their activity on putative targets POLA1 and HDACs was assessed. Initially, the ability of these compounds to target POLA1 was evaluated by performing an *in vitro* primer extension assay at increasing concentrations. ST1926 and CD437 were tested as reference compounds. Briefly, the active recombinant POLA1 drives the 10 nt extension of a primer, which results in a gel shift to a higher molecular weight extended product. The intensity of the 25-nt product (10 dNTP incorporations) is directly related to POLA1 activity. It was found that MIR002 and GEM144 showed a POLA1 primer extension inhibition at doses ranging from 10 to 50 μM, in the same range of ST1926 and CD437 (Fig. 2a).

Then, the activity profile of MIR002 and GEM144 was assessed on a panel of 11 HDAC isoforms (HDACs 1−11) by measuring the reduction of fluorescence emitted by deacetylation of a specific fluorescent substrate. In a preliminary experiment, the compounds were tested at 10 μM concentrations. Both MIR002 and GEM144 selectively inhibited HDAC11 (Fig. 2b). Furthermore, MIR002 and GEM144 were tested in a 10-dose experiment with a three-fold serial dilution starting from 10 μM (Fig. 2c). Trichostatin (TSA) was used as reference inhibitor for HDAC11 [26]. These experiments confirmed the inhibitory activity of MIR002 and GEM144 on HDAC11 (IC_{50} 6.09 μM and 8.23 μM, respectively). HDAC11, which is the most recently identified zinc-dependent HDAC, is overexpressed in several carcinomas [27] and regulates several biological processes, including immune cells differentiation [28]. Noteworthy, HDAC isoform specificity is a real challenge in this area of research, and to the best of our knowledge very few HDAC 11-selective inhibitors have been reported in the literature so far [29−31].

2.4. Molecular modelling studies on MIR002 and GEM144

Molecular modelling studies were performed to explore the binding mode of MIR002 and GEM144 analogues to POLA1 and HDAC. Concerning the POLA1 enzyme, docking calculations were carried out on the POLA1 structure co-crystallized with aphidicolin and DNA-RNA duplex (PDB Id: 4Q5V) by using the GOLD program [7]. Docking simulations were focused on the same region accommodating aphidicolin (despite the clear structural differences with the here simulated derivatives) since the derived binding pocket corresponds to the enzymatic catalytic site and all published docking studies involving POLA1 were focused on this cavity [19,32]. Fig. 2d shows the computed complex for MIR002 and reveals an arrangement which seems to be heavily influenced by the extended interactions of the hydroxamic acid group with the nucleotide bases. In fact, it reveals a pose slightly different compared to those previously observed for congeners such as ST1926, devoid of the hydroxamic tail (Fig. 2e). The interactions stabilized by MIR002 can be schematized as follows: 1) the ligand carboxylate group elicits two ion-pairs with Lys947 and Lys950; 2) the hydroxamic group has a bridging role between DNA and RNA segments since the NH−OH atoms stabilize H-bonds with the RNA C916, G917 and C918 bases, while the carbonyl group is engaged by the DNA DG920, which also contacts the ether oxygen atom; 3) the adamantyl moiety is inserted within a rather hydrophobic niche lined by both DNA bases (i.e. DC922 and DG923) and POLA1 residues (i.e. Tyr865 and Tyr957). The comparison between the

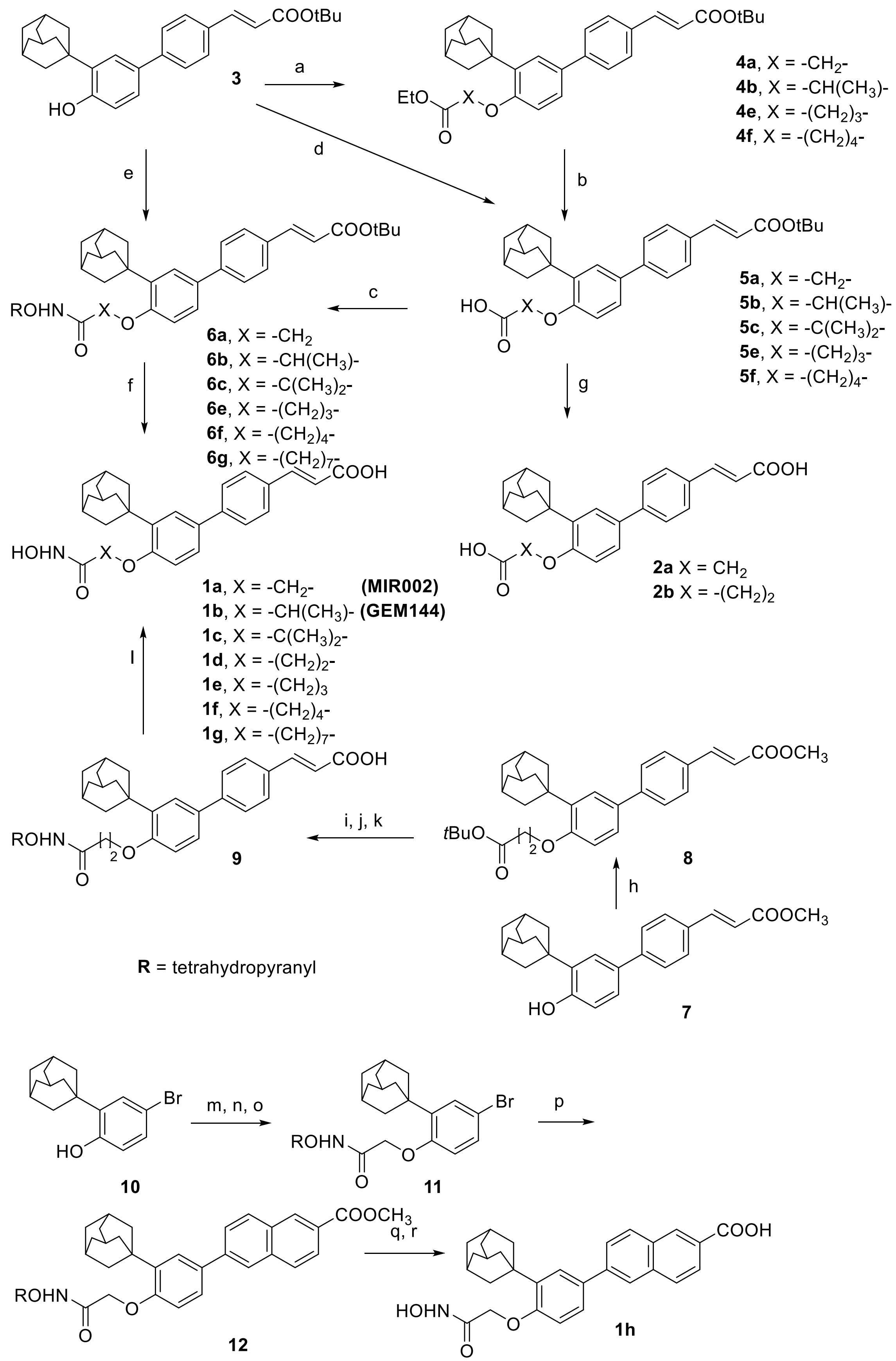
COOtBu
HO
3
a
EtO
X
O
4a, X = -CH2-
4b, X = -CH(CH3)-
4e, X = -(CH2)3-
4f, X = -(CH2)4-
d
e
b
ROHN
6a, X = -CH2
6b, X = -CH(CH3)-
6c, X = -C(CH3)2-
6e, X = -(CH2)3-
6f, X = -(CH2)4-
6g, X = -(CH2)7-
c
5a, X = -CH2-
5b, X = -CH(CH3)-
5c, X = -C(CH3)2-
5e, X = -(CH2)3-
5f, X = -(CH2)4-
f
g
COOH
HOHN
1a, X = -CH2- (MIR002)
1b, X = -CH(CH3)- (GEM144)
1c, X = -C(CH3)2-
1d, X = -(CH2)2-
1e, X = -(CH2)3
1f, X = -(CH2)4-
1g, X = -(CH2)7-
2a X = CH2
2b X = -(CH2)2
l
9
i, j, k
tBuO
COOCH3
8
h
7
R = tetrahydropyranyl
Br
m, n, o
10
11
p
12
q, r
1h

computed poses for MIR002 and ST1926 reveals that the two ligands differ for the arrangement of the biphenyl ring and the carboxylate ion, while their adamantyl moiety shows a superimposable pose, which also roughly corresponds to that of the cocrystallized aphidicolin. Finally, the polar interactions involving the nucleotides are markedly richer in MIR002 compared to ST1926, which can stabilize an H-bond with DG921 only by the 4′-hydroxy function.

The two simulated enantiomers for GEM144 reveal a very similar arrangement to the one described for MIR002. In contrast, in compound **1c** the hindrance exerted by the two methyl groups weakens all the contacts established by the hydroxamic acid, especially as it concerns those elicited by the carbonyl function.

Concerning the HDAC enzyme, docking studies were initially performed on HDAC1 isoform. Among the hundred computed poses for each ligand, no pose in which the hydroxamic acid properly coordinates the zinc ion of HDAC1 was found, indicating that all simulated ligands were unable to produce stable complexes with this HDAC isozyme. These facts can be explained by considering that HDAC1 possesses a well-known narrow binding pocket both around the cavity rim and the tunnel leading to the catalytic zinc ion [33], making it unable to suitably accommodate the here simulated molecules, which have the bulky adamantyl moiety.

In contrast, reliable poses were computed for MIR002 and GEM144 within the HDAC11 binding pocket. Fig. 2f shows the putative complex as generated for MIR002 and confirms its capacity to properly coordinate the zinc ion by a bidentate chelation, stabilized by the two oxygen atoms of the hydroxamic acid. The interactions of the hydroxamic acid are further stabilized by H-bonds involving the NH−OH atoms with His142 and His143, as well as the carbonyl oxygen atom with Tyr304. Interestingly, the bulky adamantyl moiety is inserted within a lateral sub-pocket, where it contacts a set of hydrophobic residues such as Phe37, Phe152, Leu268, and Tyr304. The two enantiomers of GEM144 show comparable poses in which the methyl group is roughly inserted within the same niche also harboring the adamantyl ring. In contrast, no pose as computed for **1c** was found able to properly coordinate the zinc ion. All these findings are in agreement with the obtained inhibitory activity profile of MIR002 and GEM144 on a panel of HDAC isoforms and POLA1.

2.5. Effect of MIR002 and GEM144 on proteins involved in the regulation of cell proliferation, DNA damage, and tumorigenesis

To elucidate the molecular significance of MIR002 and GEM144 dual activity, protein acetylation levels, proteins expression involved in cell cycle control and apoptosis were analyzed in NCI−H460 cells. Acetylation of α-tubulin and histone H4, two known markers for HDAC inhibition, was assessed upon treatment with increasing concentrations of the compounds, comparing their effects to those of SAHA, a pan-HDAC inhibitor (Fig. 3a).

NCI−H460 cells were exposed for 24 h to MIR002 and GEM144 at their IC_{20} (0.1 μM), IC_{50} (0.25 μM), and IC_{80} (0.4 μM). SAHA was used at its IC_{80} (7.4 μM).

Only a slight increase in tubulin acetylation was observed at high doses of GEM144, while no modification in H4 acetylation was noted in MIR002 and GEM144 treated cells. These results are substantially in line with the previous observations, indicating that the compounds are ineffective at least on nuclear HDAC1/2 and only marginally active on HDAC6 (GEM144). As expected, the positive control SAHA at its IC_{80} strongly enhanced both α-tubulin and H4 acetylation (Fig. 3a).

Key proteins involved in cell cycle regulation, cell proliferation, and DNA damage were also evaluated under the same conditions (Fig. 3b−c).

Cells exposed to MIR002, GEM144, and ST1926 at their respectively IC_{20}, IC_{50} and IC_{80}, strongly upregulated p21 expression in a dose-dependent manner, due to POLA1 inhibition and the related arrest in early S-Phase. SAHA treatment potently induced p21 upregulation as well, as previously reported [34].

As expected for DNA damaging agents, MIR002 and GEM144 strongly increased levels of H2AX phosphorylation on Ser 39 (γH2AX), a recognized marker of DNA damage and ATR activation. ST1926 exerted the same effect, although at a lower efficiency. SAHA increased the levels of γH2AX as well, similarly to GEM144 and MIR002. The mechanism of SAHA-induced DNA damage does not involve POLA1 inhibition and remains to be determined [35]. ERK 1/2 phosphorylation and PIN1protein levels were reduced (Fig. 4b), suggesting that these promoters of cancer-driving pathways were inhibited [36,37]. SAHA exerted similar effects on these mediators.

Interestingly, a robust induction of p53 acetylation on lysine 382 was observed exclusively in cells treated with MIR002 and GEM144. Acetylation of p53 on Lys382 correlates with an increased protein stability and activity. We hypothesized that the stronger p53 acetylation induced by MIR002 and GEM144 with respect to ST1926, could be an indirect effect of HDAC11 inhibition. In fact, HDAC11 inhibition has recently been associated with p53 expression and regulation [38]. In addition, more recently, Gong et al. [39] reported that in liver cancer cells, the expression of high levels of HDAC11 negatively correlates with the expression of p53. Further findings indicated that HDAC11 forms a complex with Egr1, the transcription factor of p53, inducing Egr1 deacetylation and thus preventing p53 gene transcription.

Furthermore, two mesothelioma cell lines (MM473 and MM487) treated with MIR002 and the ovarian carcinoma cell line A2780 treated with GEM144 were analyzed (Fig. 3c). Both compounds used at their relative IC_{20}, IC_{50}, and IC_{80}, confirmed a dose-dependent p53 acetylation and p21 induction as well as H2AX phosphorylation. However, treatment with SAHA did not induced H2AX phosphorylation.

Taken together, these results indicate that both MIR002 and GEM144 reveal substantial differences in their mechanism of action with respect to ST1926 and SAHA. Moreover, POLA1 inhibition correlates with G1-S cell cycle arrest, p21 increase, and H2AX phosphorylation. In addition, the increase in p53 acetylation exerted by MIR002 and GEM144 highlights HDAC11 as a second target for these molecules.

Scheme 1. Synthetic procedure for the preparation of compounds **1a-h** and **2a-b**. Reagents and conditions: a) K_2CO_3, DMF, $Br(CH_2)nCOOEt$, 80 °C, for **2a**: 97%, **2e**: 97%, **2f**: 76% or K2CO3, KI, 2-bromopropionic acid ethyl ester, acetone, reflux, for **2b**: 55%; b) i. LiOH·H_2O THF/H_2O 1:1 room temperature (rt), overnight; ii. 1 M $KHSO_4$, for **3a**: 98%, **3b**: 98%, **3e**: 87%; **3f**: 84%; c) i. HBTU, DIPEA, DMF, 0 °C, N2; ii. NH_2OTHP, 0 °C then rt overnight, for **4a**: 82%, **4b**: 84%, **4c**: 42%; or i. WSC, HOBt, DMF, rt, overnight, ii. NH_2OH·HCl, TEA, 3h, rt for **4f**: 45%; d) i. NaOH, MEK, 50 °C, ii. α-bromoisobutyric acid, MEK, 4h, 50 °C, 72%; e) $Br(CH_2)_7CONHOTHP$, K_2CO_3, CH_3CN/DMF, 80 °C, 43%; f) TFA, 0 °C, 1h, for **5a**: 92% or CH_2Cl_2: TFA 1:1, 0 °C, 5h, for **5b**: 64%, 5c: 69%; CH_2Cl_2: TFA 2:1, 0 °C, 2h, for **5e**: 44%, **5f**: 89%, **5g**: 100%; g) CH_2Cl_2/TFA 3.15:1, 0 °C, 2h, **9a**:79%, **9b**: 95%; h) Na, *tert*-butyl acrylate, 110 °C, 8h, N_2, 45%; i) CH_2Cl_2/TFA 3.5:1, 0 °C, 3h, N_2, 51%; j) i. HBTU, DIPEA, DMF, 0 °C, N_2; ii. NH_2OTHP, rt overnight, 93%; k) i. LiOH·H_2O THF/H_2O 1:1, rt, overnight; ii. HCl 1 M, 78%; l) 4 M HCl in dioxane, 0 °C to rt, 2h, N_2, 60%; m) K_2CO_3, DMF, $BrCH_2COOEt$, 1h, 80 °C, 62%; n) i. LiOH·H_2O THF/H_2O 1:1, rt, overnight; ii. 2 M HCl, 94%; o) i. HBTU, DIPEA, DMF, 0 °C; ii. NH_2OTHP, rt, overnight, 79%; p) $PdCl_2(dppf)\cdot CH_2Cl_2$, $NaHCO_3$, DME/H_2O 3.5:1, 6-(methoxycarbonyl)-naphthalene-2-boronic acid pinacol ester, 1h, 110 °C, 88%; q) i. 1 M NaOH in MeOH, 1h, reflux; ii. 3 M HCl,79%; r) CH_2Cl_2/TFA 3:1, 3h, 0 °C, 50%.

Table 1
Evaluation of the antiproliferative activity of the indicated POLA1/HDAC dual inhibitors in human NCI–H460 and ST1926-resistant (H460-R9A) NSCLC cells, and in A2780 and multidrug-resistant A2780-Dx ovarian carcinoma cell lines. Cells were exposed for 24 h to molecules and the anti-proliferative activity was assessed upon 48 h recovery in drug-free medium with the SRB assay. Data are expressed as $IC_{50} \pm SD$ (μM): n.e., not evaluated. RI, Resistance Index.

Compound	NCI–H460	H460-R9A	RI	A2780	A2780-DX	RI
ST1926	0.12 ± 0.002	8.4 ± 0.2	70	0.098 ± 0.001	0.17 ± 0.01	1.7
SAHA	4.2 ± 0.2	1.9 ± 0.07	0.5	2.1 ± 0.2	3.3 ± 0.6	1.6
CD437	0.22 ± 0.01	12.4 ± 0.5	56	0.21 ± 0.01	0.31 ± 0.02	1.4
1a (MIR002)	0.25 ± 0.01	2.8 ± 0.05	11.2	0.6 ± 0.01	0.41 ± 0.005	0.7
1b (GEM144)	0.26 ± 0.009	2.2 ± 0.09	8.5	0.95 ± 0.04	0.66 ± 0.01	0.7
1c	1.3 ± 0.05	7.3 ± 0.2	5.6	5.2 ± 0.1	4.2 ± 0.3	0.8
1d	8.3 ± 0.1	10.6 ± 0.3	1.3	n.e	n.e	
1e	1.7 ± 0.08	8.3 ± 0.2	4.9	4.2 ± 0.1	3.9 ± 0.4	0.9
1f	1.9 ± 0.1	8.6 ± 0.2	4.5	3.6 ± 0.2	6.4 ± 0.9	1.7
1g	5.5 ± 0.2	9.6 ± 0.3	1.7	n.e	n.e	
1h	0.65 ± 0.01	2.3 ± 0.04	3.5	n.e	n.e	
2a	>10	>50	–	n.e	n.e	
2b	10.0 ± 0.6	>50	–	10 ± 0.2	23.8 ± 0.6	2.38

Table 2
Evaluation of antiproliferative activity of MIR002 and GEM144 in the indicated cell lines. Cells were exposed for 24 h to molecules and the antiproliferative activity was assessed upon 48 h recovery in drug-free medium with the SRB assay. Data are expressed as $IC_{50} \pm SD$ (μM).

Cpd	MM432	MM473	MM487	RAMOS	L-428	U-2932	Z-138	NB4	THP-1	MDA-MB231	MDA-MB436	U87MG
ST1926	0.43 ± 0.1	0.6 ± 0.1	0.1 ± 0.02	0.29 ± 0.05	0.45 ± 0.1	0.077 ± 0.02	0.026 ± 0.04	0.1 ± .0.01	0.15 ± 0.03	1.1 ± 0.4	0.55 ± 0.08	0.53 ± 0.2
SAHA	>10	>10	8.3 ± 0.7	3.9 ± 0.7	2.3 ± 0.5	1.1 ± 0.2	0.7 ± 0.1	1.2 ± 0.04	3.9 ± 0.1	5.8 ± 2.3	3.9 ± 0.4	5.2 ± 0.8
MIR002	0.9 ± 0.08	1.2 ± 0.06	0.22 ± 0.02	0.71 ± .0.2	2.1 ± .0.6	0.52 ± 0.03	0.038 ± .0.003	0.18 ± 0.04	0.42 ± 0.02	1.9 ± 0.2	0.64 ± 0.03	1.1 ± 0.3
GEM144	1.4 ± 0.06	1.4 ± 0.2	0.73 ± 0.2	1.2 ± 0.09	3.2 ± 0.5	0.77 ± 0.1	0.16 ± 0.03	0.23 ± 0.03	0.52 ± 0.02	–	0.77 ± 0.03	1.0 ± 0.1

2.6. Effect of MIR002 and GEM144 on cell cycle and apoptosis

The effect of MIR002 and GEM144 on the cell cycle progression was explored in lung NCI–H460, ovarian A2780, and mesothelioma MM473 cancer cells. Treatment with both molecules induced pronounced changes in the cell cycle distribution (Fig. 4a).

Exposure to MIR002 and GEM144 at their IC_{50}, led to an accumulation of the cells in the early S-phase of the cell cycle, suggesting that POLA1 is the primary target of these molecules [40]. This hypothesis is supported by the finding that treatment with ST1926, a well-known POLA1 inhibitor, generated a similar cell cycle profile. A significant increase in the $SubG_1$ fraction, which presumably accounts for apoptotic events, was also observed. Treatment with SAHA, a pan HDAC inhibitor, induced G_0/G_1 cell cycle arrest [41].

Mutations in POLA1, conferring resistance to CD437 and ST1926, have been recently described [9,18]. In order to determine the molecular basis underlying the resistance to POLA1 inhibitors in ST1926 resistant H460-R9A clone, POLA1 gene was preliminarily sequenced (Supplementary Fig. 1). Sanger sequencing analysis disclosed that NCI–H460-R9A cells express the L764P mutant version of POLA1. The substitution of lysine 764 with phenylalanine is absent in the NCI-460 parental cells. The mutation, located outside the catalytic domain, has been recently linked to resistance to POLA1 inhibitors [9,18].

Furthermore, the expression of POLA1 in the POLA1-mutant cell line NCI–H460-R9A is significantly lower both at mRNA and protein levels, with respect to the parental NCI–H460 cells (Fig. 4b–c).

This observation suggests that the reduced availability of the direct target, POLA1, may exacerbate the resistance to CD437 and ST1926 observed in H460-R9A. Due to the lower resistance of R9A cells to MIR002 and GEM144 with respect to CD437 and ST1926, we wondered whether these effects mainly rely on the HDAC inhibitory activity or on their ability to hinder the mutated form of the protein. Treatment of parental H460 cells with MIR002 and GEM144 led to a reduction of wild-type POLA1 (GEM144 > MIR002), while no effects were observed on the mutated POLA1 protein level in H460-R9A.. Although the IC_{50} of GEM144 and MIR002 in H460-R9A (2.2–2.8 μM) are about 9–11 times higher than those observed in parental H460 cells (0.25 μM), the two molecules show a cytotoxic activity that is about 4 times higher than ST1926 (8.4 μM), a selective POLA1 inhibitor. We hypothesize that the combined targeting of HDAC11 and POLA1 might contribute to their higher antiproliferative effects with respect to ST1926.

An indirect confirmation of the reduced effect of MIR002 and GEM144 on mutated POLA1 derived from the analysis of the cell cycle carried out on H460-R9A cells treated at the IC_{50} of MIR002 (2.8 μM), ST1926 (8.4 μM), SAHA (1.9 μM). MIR002 at its IC_{50} didn't show any effect on cell cycle arrest in early S-phase, as expected from POLA1 inhibition (Fig. 4a). More interestingly, the compound strongly increased the $SubG_1$ fraction. On the contrary, ST1926 at its IC_{50} on H460-R9A continued to work as a POLA1 inhibitor, blocking the cells in early S-phase. According to its different mechanism of action, SAHA did not produce changes in H460-R9A cell cycle compared to H460.

In order to verify if an additive/synergistic cytotoxic activity could be obtained by simultaneous inhibition of HDAC11 and POLA1, we carried out experiments treating H460-R9A cells with SIS17 (a selective HDAC11 inhibitor) [31,42] in combination with ST1926 (a selective POLA1 inhibitor). For this purpose, the cytotoxic activity of each single compound was first calculated (Supplementary Fig. 2).). The Combination Index (CI) values of drugs were calculated at cell fraction affected (Fa) corresponding to 0.50, 0.75, and 0.90 (ED_{50}, ED_{75}, ED_{90}) (i.e. the % of cell growth inhibition) with the CalcuSyn program and expressed in terms of additive effect ($CI = 1$), synergism ($CI < 1$), or antagonism ($CI > 1$). The results revealed that when resistant cell were exposed to different concentrations of ST1926 and SIS17 (at doses corresponding about to their IC_{60}, IC_{35} and IC_{20} as single agent), the combination produced a cytotoxic effect ranging from additive to synergistic, as shown in Fig. 5.

These results can be considered a supporting evidence that the reduced resistance index to GEM144 or MIR002 with respect to

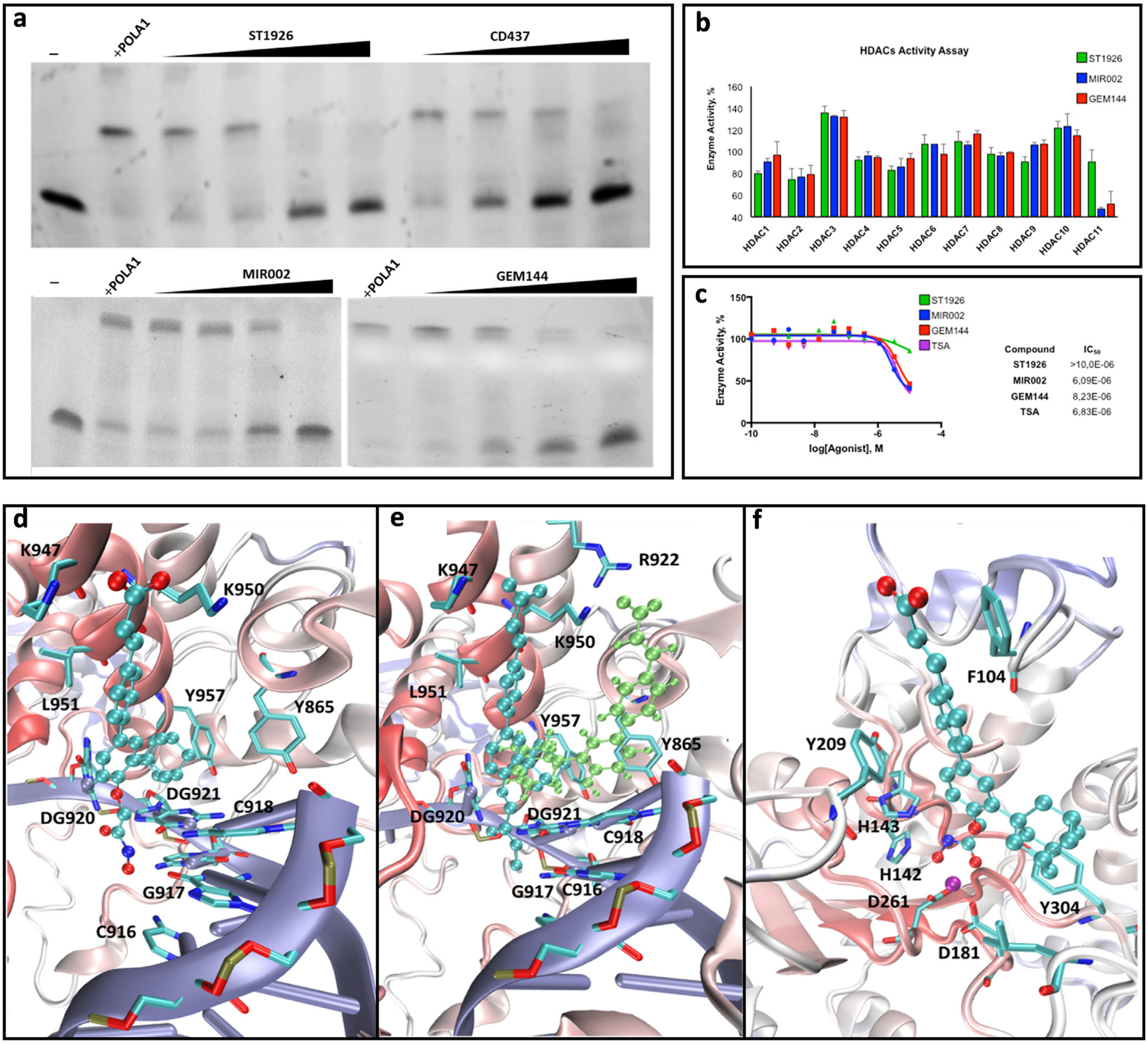

Fig. 2. Inhibition of POLA1 and HADC 11 and molecular modelling studies. (a) POLA1 primer extension inhibition was determined in the presence of increasing concentrations of ST1926, CD437, MIR002, and GEM144. (b) ST1926, MIR002, and GEM144 were tested in a single dose (10 μM) against HDACs 1–11. (c) For the evaluation of the IC_{50} the compounds were tested against HDAC11. Reactions were performed in duplicate, in a 10-dose IC_{50} mode with 3-fold serial dilution starting at 10 μM. Trichostatin A (TSA) was used as an HDAC inhibitor reference compound. IC_{50} values were calculated using the GraphPad Prism 4 program based on a sigmoidal dose-response equation. IC_{50} is reported within the panel. (d) Putative complexes as computed for MIR002 within the catalytic site of POLA1 (e) Poses for MIR002 (in cyan) and ST1926 (in lime) within the POLA1 cavity; the figure evidences the different arrangement of the biphenyl system. (f) Putative complexes as computed for MIR002 within the catalytic site of HDAC11.

ST1926 in H460-R9A carrying POLA1 mutation, is due to their dual inhibition of HDAC11/POLA1.

2.7. *In vivo* evaluation of the antitumor activity of MIR002 and GEM144

MIR002 and GEM144 were initially investigated for their pharmacokinetic parameters after single oral administration of 50, 100 and 150 mg/kg (data not shown). For both compounds, dose-dependent increases of plasma concentration were assessed. Both compounds were rapidly absorbed (Cmax at 60 min after administration) with a T1/2 of about 3 h. Due to the short half-life of both compounds, *in vivo* experiments were performed using a dose of 50 mg/kg, administered orally, twice a day (Bid) for 5 days a week, repeated 3–4 weeks (Bid 50 mg/kg, qd × 5 × 3-4w).

In the NSCLC NCI–H460 model, four days after tumor implantation, animals were divided into three groups and treated with vehicle, MIR002 (50 mg/kg using the schedule Bid, qd × 5 × 3w and ST1926 at its maximum tolerated dose (20 mg/kg, using the schedule qd × 5 × 3w). Both ST1926 and MIR002 induced a significant tumor inhibition (TGI = 61%) without any effect on body weight, indicating a good tolerability of both compounds at these doses (Fig. 6a–c).

Using the same doses and schedule (Bid; 50 mg/kg;

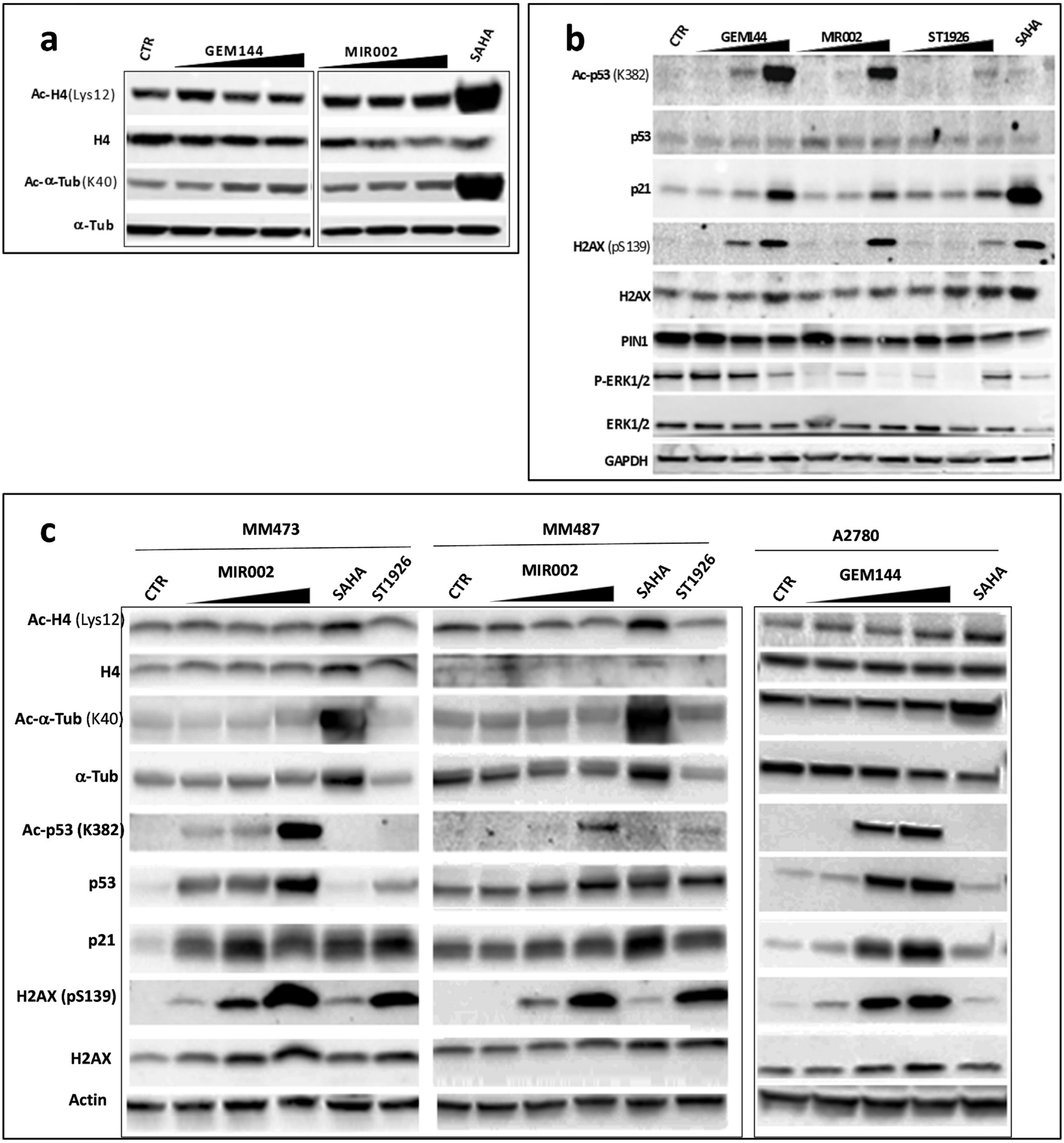

Fig. 3. (a–b) Western blot analysis of acetylated proteins, DNA damage, and signalling players in H460 lung cancer cells. (a) Levels of acetylated Histone-H4 and α–tubulin were investigated with increasing concentrations of GEM144 and MIR002 (IC_{20}, IC_{50}, IC_{80}). SAHA was used as reference compound at its IC_{80}. Ctr, untreated cells. (b) Western blot analysis performed on NCI–H460 cells treated with increasing concentations of GEM144 and MIR002 (IC_{20}, IC_{50}, IC_{80}) while ST1926 and SAHA were used at their IC_{80}. Ctr, untreated cells. GAPDH was used as a loading control. (c) Protein expression analysis by Western blot in two mesothelioma cell lines (MM473 and MM487) and ovarian cancer cells (A2780) treated with the compounds as previous described in b). Ctr, untreated cells. The results are representative of three independent experiments.

a

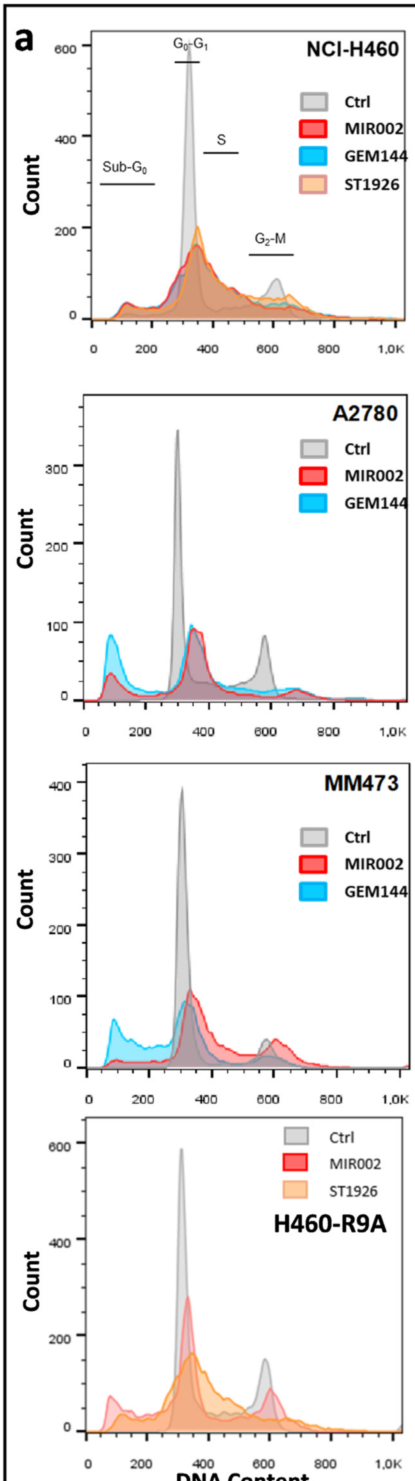

Cell line: NCI-H460	Sub-G_1	$G_{0/1}$	S	G_2/M
Control	1.1	46.8	32.1	21.1
MIR002	12.1	16.3	80.9	2.8
GEM144	13.2	10.9	81.4	7.8
ST1926	12.4	13.8	79.7	6.5
SAHA	1.8	65.2	11.7	23.1

Cell line: A2780	Sub-G_1	$G_{0/1}$	S	G_2/M
Control	1.6	48.7	36.3	15
MIR002	33.3	14.6	78.9	6.5
GEM144	23	10.8	86.2	3

Cell line: MM473-Luc	Sub-G_1	$G_{0/1}$	S	G_2/M
Control	1.3	74.7	13.7	11.7
MIR002	39.7	23	62.9	14.1
GEM144	10.2	2.3	81.6	16.1

Cell line: H460-R9A	Sub-G_1	$G_{0/1}$	S	G_2/M
Control	1.5	50.1	34.5	15.4
MIR002	37.8	49.7	37.4	12.9
ST1926	26.7	22.8	63.4	13.8
SAHA	2.1	62.2	14.7	21.0

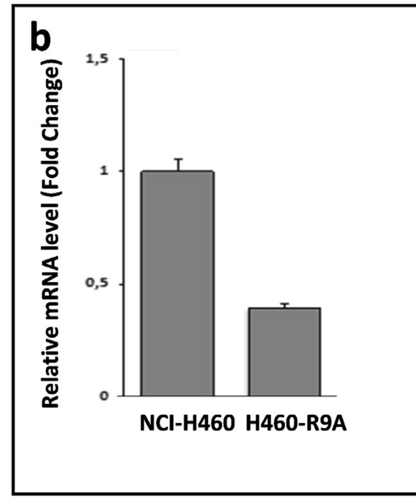

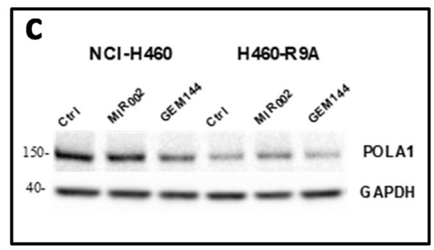

Fig. 4. Cell cycle analysis after MIR002 and GEM144 exposure in different cancer cell lines. (a) NCI–H460, A2780 and MM473, H460-R9A cell lines were treated for 72 h with the compounds at their IC_{50}. ST1926 and SAHA were used as reference in some tests; Cells were stained with PI, and processed on a FACScan flow cytometer to assess cell cycle distribution and apoptosis (SubG1 fraction). (b) Quantitative RT-PCR analysis of POLA1 mRNA levels in H460 and H460-R9A cells. The bar graph shows the normalized levels of POLA1 mRNA as fold changes with respect to parental cells, represented as average±SEM of three independent experiments. (c) Western blot analysis of POLA1 protein levels in cells treated with IC_{50} MIR002 and GEM144 for 24 h. Ctr, vehicle-treated cells, GAPDH was used for normalization.

a

	Concentrations (μM)					
ST1926	0	0.75	1.5	3	6	12
SIS17	0	3.75	7.5	15.0	30.0	60.0
ST1926+SIS17	0	0.75 + 3.75	1.5 + 7.5	3 + 15	6 + 30	12 + 60

b

	OD (mean values ± SD)					
CTR	1.424 ± 0.255					
ST1926	0	1.420± 0.192	1.299± 0.103	1.147± 0.067	1.000± 0.157	0.577± 0.075
SIS17	0	1.412± 0.082	1.399± 0.120	1.177± 0.057	0.964± 0.199	0.457± 0.082
ST1926+SIS17	0	1.410± 0.123	1.307± 0.095	0.959± 0.125	0.528± 0.129	0.228± 0.058

c

Fa	CI	Effect
ED_{50}	1.09	Nearly additive
ED_{75}	0.87	Slight synergism
ED_{90}	0.69	Synergism

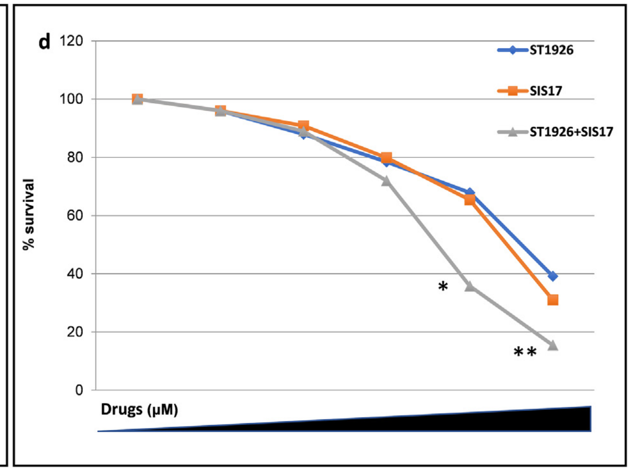

Fig. 5. Antiproliferative effect of ST1926, SIS17 and their combination in H460-R9A cell line. (a) Human H460- R9A NSCLC cells were exposed to increasing concentrations of ST1926 and SIS17, alone and in combination. (b) Cell sensitivity to the compounds assessed upon 72 h with the MTT assay. (c) Combination Index (CI) values of drugs were calculated at cell fraction affected (Fa) of 0.50, 0.75, and 0.90 (ED_{50}, ED_{75}, ED_{90}) (i.e. the % of cell growth inhibition) with the CalcuSyn program and expressed the combination of ST1926 plus SIS17 with respect to the single drug, in terms of additive effect (CI = 1), synergism (CI < 1), or antagonism (CI > 1). (d) The % survival was evaluated by using formula: % = 100 × (OD Drug(s)/OD CTR control). Statistical analysis was performed using the OD data (b) of ST1926+SIS17 combination versus the single drugs with 1-way ANOVA followed by Bonferroni post hoc correction (*p < 0.001; **p < 0.0001).

qd × 5 × 4w), MIR002 was investigated in comparison with ST1926 (20 mg/kg) and in association to cisplatin (i.p. 5 mg/kg; q7d × 4w) in the ST1926-resistant NCI—H460-R9A tumor cells xenografted in nude mice (Fig. 6d—f). Interestingly, while ST1926 was completely ineffective, MIR002 showed the same antitumor activity of cisplatin (TGI = 38%), even if lower than the activity on the parental NCI—H460 cells (Fig. 6d—e).

An unexpected finding was the outstanding efficacy of the combination of MIR002 with cisplatin, reaching a TGI>78%, with two animals (2/8) without any measurable tumors at the end of experiment. Moreover, the administration of MIR002 did not show any side effect on mice body weight also in combination with cisplatin, thus suggesting again a good tolerability of this compound.

In a xenografted mesothelioma MM473 orthotopic model, MIR002 administered orally at 50 mg/kg (Bid, qd × 5 × 3 weeks) gave a 77% of TGI versus vehicle (Supplementary Fig. 3).

By using the same doses and a more prolonged schedule (Bid, qd × 5 × 6w), GEM144 was investigated in a MM487 biphasic model in comparison to cisplatin (i.p. 5 mg/kg; q7d × 6w) (Fig. 7a—c). Confirming the antitumor activity, GEM144 significantly reduced tumor burden of MM487 (TGI = 72%), while treatment with the standard-of-care (cisplatin) showed a lower activity (42%). The low efficacy of cisplatin may have been the cause that led to sacrifice two animals in this group as well as in the control group for ethical reasons before the end of experiment.

2.8. *Evaluation of IFNα level in immunocompetent mice xenografted with B16 mouse melanoma cells*

Recently, a link between POLA1 and type I interferons has been described while studying the etiology of X-linked reticulate pigmentary disorder (XLPDR), a primary immunodeficiency with autoinflammatory features [6]. The mutation which disrupts the expression of POLA1, resulted in increased production of type I interferons. In addition, recent literature data revealed the roles of HDAC11 not only in the development of different cancer types [43], but also in the regulation of type I interferon signaling and different immune cells including neutrophils, myeloid derived suppressor cells, and T-cells [44,45].

Therefore, we examined whether a direct inhibition of POLA1 and HDAC11 by MIR002 could lead to an increase in interferons production. Ten immunocompetent C57/Bl6 mice were transplanted with syngeneic melanoma cells (B16 mouse melanoma cells). After 10 days from tumor implant (average tumor volumes were 320 mm^3), mice were divided into two groups and treated orally with MIR002 (5 mice, 50 mg/kg, twice a day for 5 days) or vehicle (5 mice). Five hours after the last administration, plasma was collected and analyzed by ELISA kit for the α interferon detection. Plasma analysis revealed that mice treated with MIR002 significantly increased their α interferon levels, showing a double concentration compared to the control group (1200 *vs* 500 pg/mL, respectively) (Supplementary Fig. 4).

A recent finding demonstrated that POLA1 deficiency resulted in increased production of type I interferons [6], since POLA1 loss of function was associated with the generation of cytosolic RNA-DNA hybrids and to the activation of innate immune sensors as type I interferons. Therefore, we investigated whether the inhibition of POLA1 by MIR002 could have the same effect in promoting interferon production. Our results in B16 model revealed that after only a five-day treatment, MIR002 induced a significant increase of α interferon at its pharmacological active dose (Bid, 50 mg/kg). This is particularly interesting taking into account the remarkable antitumor preclinical and clinical effects of class I interferons [46] and their ability to activate host immune responses [47—50].

3. Conclusions

In this study, we investigated the antitumor activity of a set of new molecules, designed with the aim to target simultaneously POLA1 and HDACs. Two molecules, MIR002 and GEM144 were selected for their antiproliferative activity on a wide panel of human tumor cell lines. Further *in vitro* functional assays revealed that these molecules potently inhibit POLA1 and specifically, among known HDACs, inhibit HDAC11.

Our data pinpointed that MIR002 and GEM144 possess substantial differences in their mechanism of action with respect to their cognate analogue ST1926 and the pan-histone deacetylase inhibitor SAHA. Similarly to ST1926, our dual inhibitors target POLA1. However, the differences in mechanism of action become evident when their activities were compared to the ST1926-resistant lung cancer H460-R9A cells. In fact, this cell line

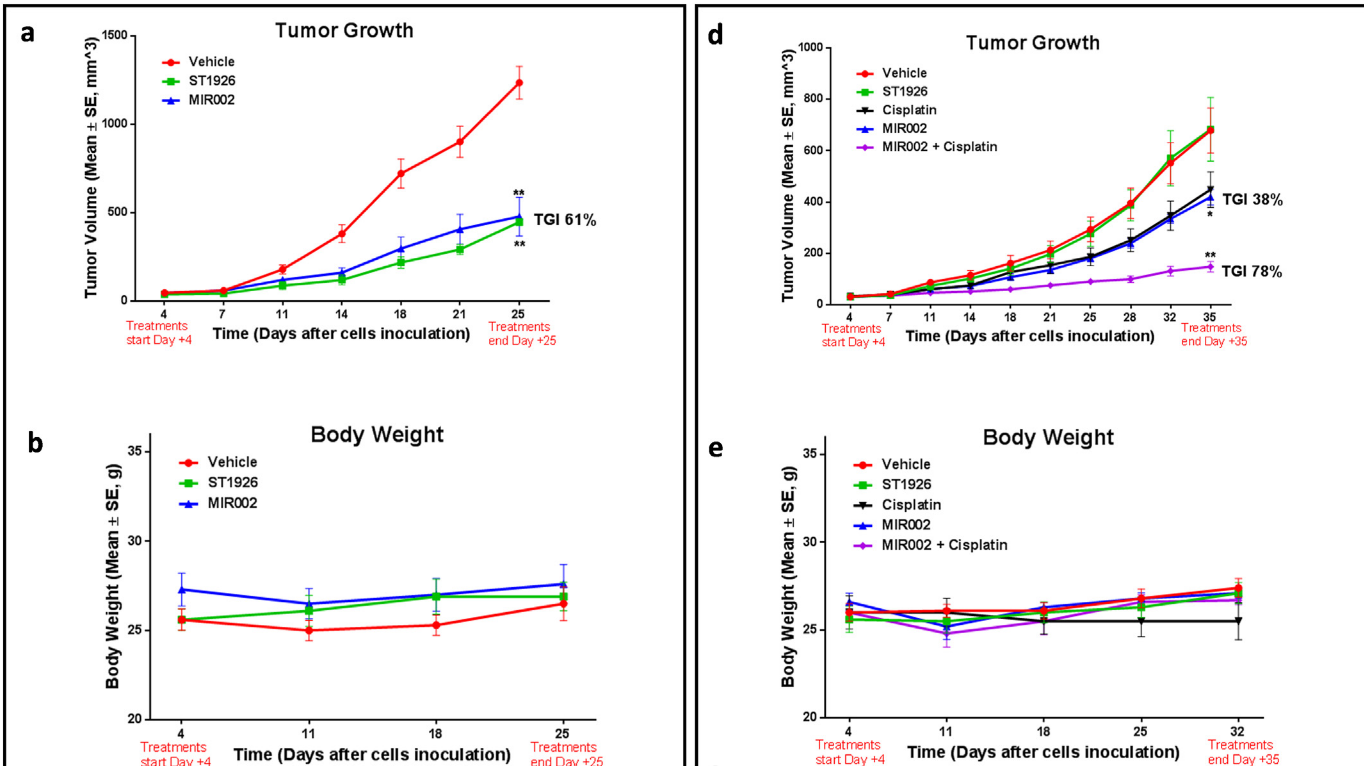

c

Administered Compounds	Route of Administration	Dose	Schedule	BWL Day +25 (%)	TGI Day +25 (%)
Vehicle	OS	-	bid, qdx5/wx3w	0	-
ST1926	OS	20 mg/kg	q2dx3/wx3w	0	64
MIR002	OS	50 mg/kg	bid, qdx5/wx3w	0	61

f

Administered Compounds	Route of Administration	Dose	Schedule	BWL Day +35 (%)	TGI Day +35 (%)
Vehicle	OS + IV	-	bid, qdx5/wx4w q7dx4w	0	-
ST1926	OS	20 mg/kg	q2dx3/wx4w	0	0
Cisplatin	IV	4 mg/kg	q7dx4w	2,4	34
MIR002	OS	50 mg/kg	bid, qdx5/wx4w	0	38
MIR002 + Cisplatin	OS + IV	50 mg/kg 4 mg/kg	bid, qdx5/wx4w q7dx4w	0	78

Fig. 6. *In vivo* antitumor activities of MIR002 and GEM144. (a) H460, mean tumor volume and (b) body weight variation throughout the experimental period. (c) Summary table. (d) H460-R9A retinoid resistant cells, mean tumor volume (d) and body weight variation (e) throughout the experimental period. (f) Summary table.

expressing the POLA1 mutant version (L764P) of POLA1 is highly resistant to POLA1 inhibitor ST1926 (R.I. = 70), while it shows a low resistance towards MIR002 and GEM144 (RI < 10). Our biochemical and molecular analysis indicated that the resistance to ST1926 as well as to CD437 was due to the significant reduction in POLA1 expression. We suggest that the lower POLA1 expression in this cell line, which reduced the possibility of drug-POLA1 interaction, led to a low level of DNA damage, not enough to activate apoptotic pathways. According to this hypothesis, dual molecules were less sensitive to POLA1 reduction because they could overcome H460-R9A resistance by acting via HDAC11 inhibition, which ultimately led to the activation of apoptotic pathways.

Further evidence was derived from *in vivo* experiments in the NCI−H460 and NCI−H460-R9A models. In fact, whereas MIR002 and ST1926 inhibited tumor growth of NCI−H460 with similar potency, ST1926 was completely ineffective in the NCI−H460-R9A model. It is important to highlight the efficacy of MIR002 in combination with cisplatin in the NCI−H460-R9A model. Moreover, MIR002 and GEM144 showed significant *in vivo* antitumor activity in two human malignant pleural mesothelioma cell lines (MM473 and MM487) stably transfected with luciferase and orthotopically xenografted in nude mice. The only standard initial treatment for unresectable malignant pleural mesothelioma is combination chemotherapy with cisplatin and pemetrexed. Further, cisplatin/pemetrexed is the only approved regimen with evidence of prolonged overall survival (OS), although the median OS for patients treated with this regimen is only 12 months after diagnosis [51]. The robust antitumoral activity of MIR002 in combination with cisplatin could become a new efficacious pharmacological strategy to treat patients affected by tumors such as malignant pleural mesothelioma in which the response to standard therapy is ineffective.

In summary, we have identified new dual POLA1-HDAC11 inhibitors endowed with a broad spectrum of antiproliferative activities at nanomolar concentrations on a panel of cancer cell lines. Selected molecules induced acetylation of p53, activation of p21, G1/S cell cycle arrest, and apoptosis. Additionally, the compounds showed promising immunomodulatory properties, inducing a significant increase of α interferon. The broad spectrum of antitumor

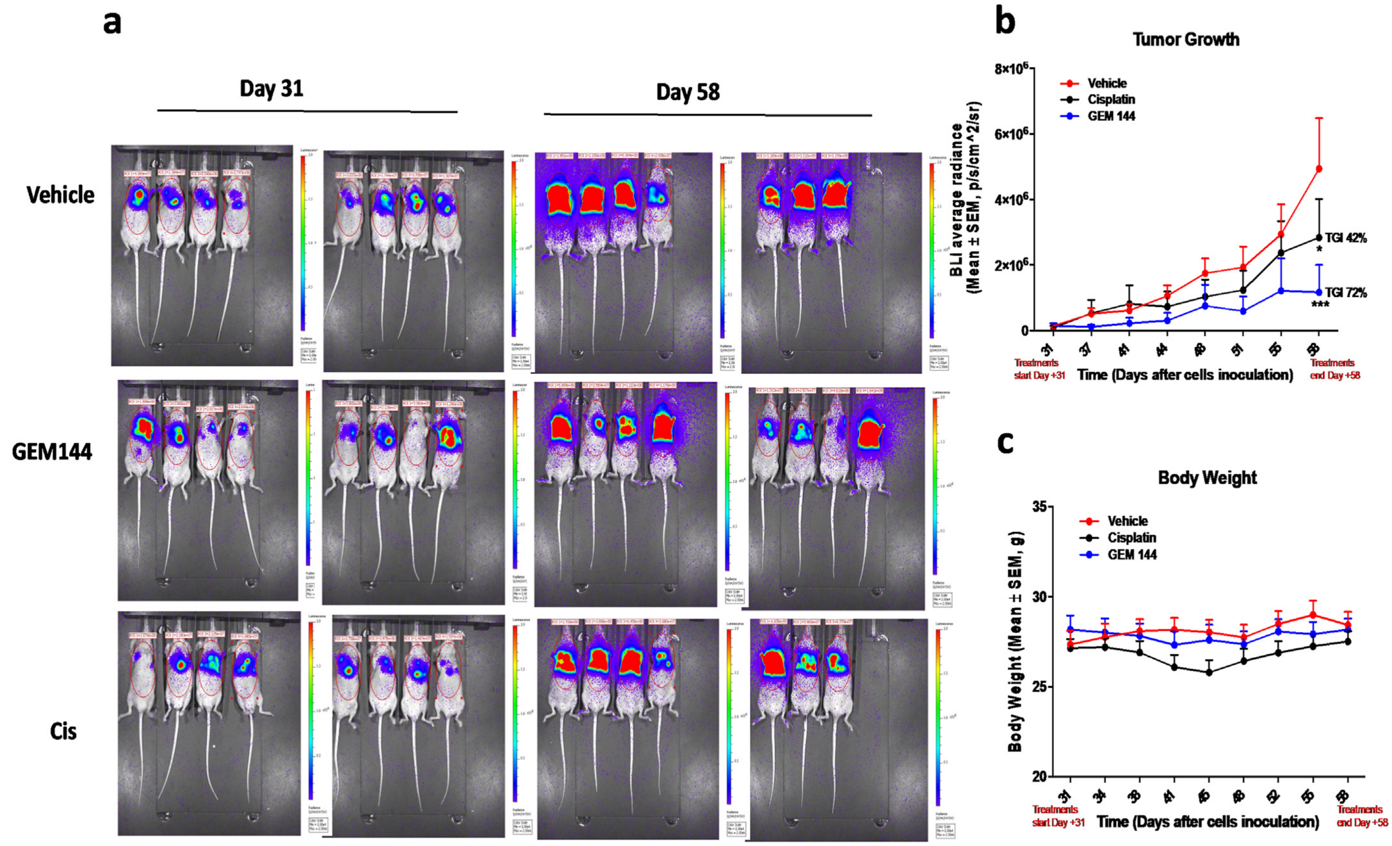

Fig. 7. *In vivo* efficacy of GEM144 in an orthotopic model of Human Malignant Pleural Mesothelioma (MM487) (a). IVIS acquisitions of eight mice/group at day 31 (Day+1 of treatments) and at day 58 (end of treatments); (b) Mean tumor bioluminescence and (c) body weight variation throughout the experimental period; Mean. *p < 0,05; ***p < 0,001.

activities in *in vivo* models opens the possibility of a future clinical investigation of the new compounds.

4. Experimental section

4.1. Chemistry-general methods

All reagents and solvents were reagent grade or were purified by standard methods before use. Melting points were determined in open capillaries by a SMP3 apparatus and are uncorrected. ^{1}H and ^{13}C spectra were recorded on Varian Mercury 300 MHz and Bruker AV600 spectrometers. Chemical shifts were reported in parts per million. The peak patterns are indicated as follows: *s*, singlet; *d*, doublet; *dd*, doublet of doublet; *t*, triplet; *m*, multiplet; *q*, quartet. The coupling constants, *J* are reported in Hertz (Hz). Solvents were routinely distilled prior to use; anhydrous tetrahydrofuran (THF) and ether (Et_2O) were obtained by distillation from sodium-benzophenone ketyl; dry methylene chloride was obtained by distillation from phosphorus pentoxide. All reactions requiring anhydrous conditions were performed under a positive nitrogen flow and all glassware were oven dried. Isolation and purification of the compounds were performed by flash column chromatography on silica gel 60 (230–400 mesh). Analytical thin-layer chromatography (TLC) was conducted on TLC plates (silica gel 60 F254, aluminium foil). Compounds on TLC plates were detected under UV light at 254 and 365 nm or revealed spraying with 10% phosphomolybdic acid (PMA) in ethanol.

The elemental analyses were recorded on a CARLO ERBA EA 1108 instrument. Analyses indicated by the symbols of the elements or functions were within ±0.4% of the theoretical values.

The purity of final compounds was determined by analytical HPLC and was found to be ≥ 95% pure. Analysis of sample purity was performed on a YL9100 HPLC System, Capcell PAK C-18, (250*4.6 mm, 4.6 μm) column. HPLC conditions: solvent A, Water +0.1% Acetic acid; solvent B, CH_3CN; flow rate, 1 mL/min.

4.2. Synthesis of compound 1a (MIR002)

4.2.1. 3-(3′-Adamantan-1-yl-4′-ethoxycarbonylmethoxybiphenyl-4-yl)acrylic acid tert-butyl ester (4a)

A mixture of compound 3 (2.00 g, 4.64 mmol) [52], ethyl bromoacetate (1.58 g, 9.28 mmol), K_2CO_3 (2.57 g, 18.6 mmol) in anhydrous DMF (40 mL) was heated at 80 °C for 1 h under nitrogen atmosphere. K_2CO_3 was filtered, the solvent was removed in vacuo and the crude diluted with water. The precipitate was filtered and crystallized from diethyl ether to give 2.09 g (yield: 97%) of the product as white solid, m.p. 175 °C, R_f(petroleum ether/ethyl acetate 90:10) 0.31.^{1}H-NMR (300 MHz, $CDCl_3$): δ 7.61 (1H, d, J= 15.9 Hz), 7.58-7.53 (4H, m), 7.50 (1H, d, J= 2.3 Hz), 7.39 (1H, dd, J= 8.4 Hz, J= 2.3 Hz), 6.79 (1H, d, J= 8.4 Hz), 6.38 (1H, d, J= 15.9 Hz), 4.67 (2H, s), 4.31 (2H, q, J= 7.2 Hz), 2.23-2.07 (9H, m), 1.88-1.74 (6H, m), 1.54 (9H, s), 1.32 (3H, t, J= 7.2 Hz).^{13}C-NMR (75 MHz, $CDCl_3$): 168.7, 166.4, 156.7, 143.2, 142.9, 139.2, 133.2, 132.9, 128.4 (× 2C), 127.1 (× 2C), 126.0, 125.2, 119.6, 112.2, 80.4, 65.4, 61.3, 40.5 (× 3C), 37.2, 37.0 (× 3C), 29.1 (× 3C), 28.2 (× 3C), 14.2.

4.2.2. 3-(3′-Adamantan-1-yl-4′-carboxymethoxybiphenyl-4-yl) acrylic acid tert-butyl ester (5a)

To a solution of **4a** (2.08 g, 4.02 mmol) in aq. 50% THF (125 mL), $LiOH·H_2O$ (843 mg, 20.1 mmol) was added and the reaction was stirred overnight at room temperature (rt). The solvent was evaporated, the residue was dissolved in EtOAc, washed with 1 N $KHSO_4$ (60 mL), and dried over anhydrous Na_2SO_4. The solvent was removed to give 1.92 g (yield: 98%) of compound **5a** as a white solid, m.p.> 300°C, R_f(CH_2Cl_2/CH_3OH 19: 1) 0.23.^{1}H-NMR (300MHz, DMSO-d_6): δ 7.75-7.60 (4H, m), 7.56 (1H, d, J= 15.8 Hz), 7.48 (1H, dd, J= 8.51 Hz, J= 2.4 Hz), 7.43 (1H, d, J= 2.4 Hz), 6.93 (1H, d, J= 8.5 Hz), 6.51 (1H, d, J= 15.8 Hz), 4.70 (2H, s), 2.19-1.98 (9H, m), 1.83-1.66 (6H, m), 1.48 (9H, s).^{13}C-NMR (75MHz, DMSO-d_6): 170.4, 166.1, 157.2,143.7, 142.5, 138.6, 132.9, 132.1, 129.3 (× 2C), 127.0 (× 2C), 125.5, 125.2, 119.7, 113.5, 80.3, 65.3, some signals are missing due to the overlap with solvent, 37.1, 37.9, 28.9 (× 3C), 28.3 (× 3C).

4.2.3. 3-{3′-Adamanan-1-yl-4′-[(tetrahydropyran-2-yloxycarbamoyl)methoxy]biphenyl-4-yl}-acrylic acid tert-butyl ester (**6a**)

To an ice-cooled suspension of compound **5a** (1.25 g, 2.56 mmol) in anhydrous DMF (26 mL), HBTU (0.971 g, 2.56 mmol) and DIPEA (0.993 g, 7.68 mmol) were added under nitrogen. After 2 min O-(tetrahydropyran-2-yl)-hydroxylamine (0.312 g, 2.56 mmol) was added and the mixture was stirred overnight at rt. The solvent was evaporated, the residue was diluted with water and the white solid filtered. The crude was purified by flash chromatography with petroleum ether/EtOAc 7:3 gave 1.23 g (yield: 82%) of compound **6a** as a white solid, m. p. 193 °C, Rf (AcOEt/petroleum ether 3:7) 0.31. ^{1}H NMR (300 MHz, $CDCl_3$): δ 9.13 (1H, s), 7.61 (1H, d, *J* = 16.0 Hz), 7.58-7.54 (4H, m), 7.51 (1H, d, *J* = 2.2 Hz), 7.43 (1H, dd, *J* = 8.5 Hz, *J* = 2.24 Hz), 6.91 (1H, d, *J* = 8.5 Hz), 6.39 (1H, d, *J* = 16.0 Hz), 5.07-5.02 (1H, m), 4.68 (2H, s), 4.00-3.90 (1H, m), 3.67-3.57 (1H, m), 2.18-2.11 (9H, m), 1.92-1.78 (8H, m), 1.70-1.58 (4H, m), 1.54 (9H, s). ^{13}C NMR (75 MHz, $CDCl_3$): 166.4, 165.1, 156.1, 143.1, 142.5, 138.8, 134.2, 133.2, 128.4 (× 2C), 127.1 (× 2C), 126.2, 125.6, 119.8, 113.4, 102.8, 80.5, 67.6, 62.5, 41.1 (× 3C), 37.1, 37.0 (× 3C), 28.9 (× 3C), 28.2 (× 3C), 27.9, 24.9, 18.5.

4.2.4. 3-(3′-Adamantan-1-yl-4′-hydroxycarbamoylmethoxybiphenyl-4-yl)acrylic acid (**1a, MIR002**)

Compound **6a** (250 mg, 0.425 mmol) was added portion wise to TFA (3.5 mL) at 0 °C under nitrogen and the mixture was stirred 1h at 0 °C. The pink suspension was filtered, the solid was washed with water until neutral pH to give 175 mg (92%) of the desired compound as a white solid, m.p. 265 °C, R_f(CH_2Cl_2/ MeOH 18: 2) 0.49.^{1}H-NMR (300 MHz, $CDCl_3$+TFA): δ 7.91 (1H, d, J = 16.0 Hz), 7.67-7.59 (4H, m), 7.55 (1H, d, J = 2.2 Hz), 7.47 (1H, dd, J= 8.3 Hz, J= 2.2 Hz), 6.90 (1H, d, J= 8.3 Hz), 6.49 (1H, d, J= 16.0 Hz), 4.78 (2H, s), 2.20-2.10 (9H, m), 1.91-1.72 (6H, m).^{13}C-NMR (75 MHz, DMSO-d_6): 168.1, 164.8, 157.7, 144.0, 142.6, 139.0, 133.1, 132.4, 129.3 (×2C), 126.8 (×2C), 125.6, 125.2, 118.9, 114.2, 66.4, 3C missing due to the overlap with signal solvent, 37.1 (×2C), 36.9 (×2C), 28.9 (×3C). Anal. calcd. for $C_{27}H_{29}NO_5$: C,72.46; H,6.53; N,3.13. Found: C,72.25; H,6.52; N,3.12.

4.3. Synthesis of compound **1b** (**GEM144**)

4.3.1. 3-[3′-Adamantan-1-yl-4'-(1-ethoxycarbonylethoxy)biphenyl-4-yl]-acrylic acid tert-butyl ester (**4b**)

To a solution of compound 3 (500 mg, 1.16 mmol) [52] in dry acetone (7 mL), K_2CO_3 (641 mg, 4.64 mmol), KI (13 mg, 0.08 mmol) and 2-bromo-propionic acid ethyl ester (180 μL, 1.39 mmol), were added under nitrogen. The mixture was heated 5 h to reflux. K_2CO_3 was filtered, and the solvent removed in vacuo. The crude was triturated with hexane: diethyl ether 5:1, the precipitate was filtered to give 340 mg of the title compound. Yield: 55%. m.p. 88 °C, R_f(petroleum ether/ethyl acetate 92.5:7.5) 0.30.^{1}H-NMR (300 MHz, $CDCl_3$):δ7.61 (1H, d, J = 15.7 Hz), 7.57-7.52 (4H, m), 7.49 (1H, d, J = 2.3 Hz), 7.35 (1H, dd, J = 2.3, 8.4 Hz), 6.71 (1H, d, J = 8.4 Hz), 6.38 (1H, d, J = 15.7 Hz), 4.88 (1H, q, J = 6.6 Hz), 4.22 (2H, q, J = 7.1 Hz), 2.31-2.14 (6H, m), 2.13-2.04 (3H, m), 1.84-1.74 (6H, m), 1.71 (3H, d, J = 6.6 Hz), 1.54 (9H, s), 1.25 (3H, t, J = 7.1 Hz).

4.3.2. 3-[3′-adamantan-1-yl-4'-(1-carboxyethoxy)biphenyl-4-yl] acrylic acid tert-butyl ester (**5b**)

To a solution of **4b** (500 mg, 0.94 mmol) in aq. 50% THF (30 mL), LiOH·H_2O (198 mg, 4.71 mmol) was added. The solution was stirred overnight at rt. The solvent was evaporated, the crude was diluted in 1 N $KHSO_4$ and extracted with EtOAc. The combined organic extracts were washed with brine, dried over anhydrous Na2SO4 and concentrated in vacuo, to give 462 mg (98%) of 3-[3′-adamantan-1-yl-4'-(1-carboxyethoxy)biphenyl-4-yl]acrylic acid *tert*-butyl ester **5b** (white solid), m. p. 206 °C, Rf (CH_2Cl_2/MeOH 193 : 7) 0.23. ^{1}H NMR (300 MHz, DMSO-d_6) δ: 7.76-7.60 (m, 4H), 7.56 (d, 1H, *J* = 15.9 Hz), 7.47 (dd, 1H, *J* = 2.0, 8.4 Hz), 7.43 (d, 1H, *J* = 2.0 Hz), 6.80 (d, 1H, *J* = 8.4 Hz), 6.51 (d, 1H, *J* = 15.9 Hz), 4.91 (q, 1H, *J* = 6.5 Hz), 2.24−2.00 (m, 9H), 1.79-1.66 (m, 6H), 1.57 (d, 3H, *J* = 6.5 Hz), 1.47 (9H, s).

4.3.3. 3-{3′-Adamantan-1-yl-4'-[1-(tetrahydropyran-2-yloxycarbamoyl)ethoxy]biphenyl-4-yl}-acrylic acid tert-butyl ester (**6b**)

To a solution of compound **5b** (400 mg, 0.79 mmol) in dry DMF (6 mL), HBTU (302 mg, 0.79 mmol) and DIPEA (423 μL, 2.38 mmol) were added at 0 °C under nitrogen atmosphere. The solution was stirred 30 min at 0 °C, then *O*-(tetrahydropyran-2-yl)-hydroxylamine (93 mg, 079 mmol) was added and the reaction was stirred overnight at rt. The solvent was removed in vacuo, the residue was triturated with water and filtered. The crude was purified by flash column chromatography in hexane: ethyl acetate 3: 1 to give 400 mg of compound **6b**. Yield: 84%, m.p. 99.5°C, R_f(hexane: ethyl acetate 7: 3) 0.32.^{1}H-NMR (300 MHz, $CDCl_3$) mixture of stereoisomer: δ 8.98 (1H, s), 8.87 (1H, s), 7.61 (2H, d, J = 15.8 Hz), 7.57-7.53 (8H, m), 7.51 (2H, d, J = 2.3 Hz), 7.45-7.35 (2H, m), 6.91-6.83 (2H, m), 6.38 (2H, d, J = 15.9 Hz), 5.03-4.81 (4H, m), 3.90-3.76 (2H, m), 3.64-3.54 (1H, m), 3.50-3.38 (1H, m), 2.26-2.07 (18H, m), 1.84-1.76 (12H, m), 1.69-1.74 (6H, m), 1.54 (18H, s).

4.3.4. 3-[3′-adamantan-1-yl-4'-(1-hydroxycarbamoylethoxy) biphenyl-4-yl]-acrylic acid (**1b, GEM144**)

To a solution of **6b** (1.35 g, 2.20 mmol) in dry CH_2Cl_2 (22 mL) at 0 °C, TFA (22 mL) was added dropwise under nitrogen. The solution was stirred at 0 °C for 4 h. The mixture was evaporated and treated with toluene to remove TFA; the solid obtained was triturated in CH_2Cl_2 and filtered to give 646 mg of compound **1b**. Yield: 64%., m.p.171.8°C, R_f (CH_2Cl_2/ MeOH/ H_2O 18: 2: 0.2) 0.35.^{1}H-NMR (300 MHz, $CDCl_3$+TFA): δ 7.92 (1H, d, J = 15.9 Hz), 7.68-7.59 (4H, m), 7.57 (1H, d, J = 2.2 Hz), 7.44 (1H, dd, J = 2.2 Hz, 8.3 Hz), 6.80 (1H, d, J = 8.3 Hz), 6.49 (1H, d, J = 15.9 Hz), 5.10-4.95 (1H, m), 2.28-2.03 (9H, m), 1.91-1.68 (9H, m).^{13}C-NMR (150 MHz, DMSO-d_6) δ : 167.6(×2C); 156.2; 143.6; 142.1; 138.1; 132.5; 131.5; 128.8 (×2C); 126.6 (×2C); 125.0 (×2C); 118.6; 113.0; 71.1; 3C missing due to the overlap with signal solvent; 36.6 (×4C);28.4 (×3C);18.8. Anal. calcd. for $C_{28}H_{31}NO_5$: C,72.86; H,6.77; N,3.03. Found: C,73.05; H,6.76; N,3.03.

The synthesis of compounds **1c-1h**, **2a-b** is reported in the Supporting information.

4.4. Cell lines

Human NCI−H460 (# HTB-177) NSCLC, MDA-MB436 (# HTB130) breast carcinoma, JECO-1 (# CRL-3006), and Z-138 (# CRL-3001) mantle cell lymphoma were acquired from the American Type Culture Collection (ATCC). A2780 (# 93112519) and A2780-Dx (# 93112520) multidrug-resistant ovarian carcinoma, HT29 (# 91072201) and HCT116 (# 91091005) colorectal carcinoma were from the European Collection of Authenticated Cell Cultures (ECACC).

MAVER-2 (# ACC-717), MINO (# ACC-687), REC-1 (# ACC-584), mantle cell lymphoma; U937 (# ACC-5) histiocytic lymphoma; RAJI (# ACC-319), DG-75 (# ACC-83) and RAMOS (# ACC-603) Burkitt lymphoma; KM-H2 (# ACC-87) and L-428 (# ACC-197) Hodgkin lymphoma; OCI-LY3 (# ACC-731) and U-2932 (# ACC-633) diffuse large B-cell lymphoma; NB4 (ACC-207) pro-myelocytic leukemia (APL) were from the German Collection of Microorganisms and Cell Cultures (DSMZ). U87MG-Luc glioma was from Caliper Life Sciences.

H460-R9A cell line was a ST1926-resistant H460 subline, isolated after exposure at increasing doses of ST1926 [25].

Mesothelioma Cells: MM487 (biphasic pleural mesothelioma) and MM473 (epithelioid pleural mesothelioma) were isolated in Alessandria hospital (Italy) from two patients affected by pleural mesothelioma [53].

Luciferase-expressing human mesothelioma cells: MM473 and MM487 mesothelioma cells were stably transfected with pGL4.17 pWHERE CMV luc vector. Forty-eight hours after transfection, cells were cultured for three weeks in neomycin-containing (400 μg/mL, Gibco, USA) Ham's F-10 Nutrient Mixture medium (Gibco, USA). Neomycin-resistant colonies were isolated using cloning rings and transferred into 96-well plates for expansion. Evaluation of luciferase expression was performed by seeding serially diluted clones into 96-well plates (ranging from 0.1×10^3 to 1×10^5 cells/well). Upon incubation with D-Luciferin (Perkin-Elmer), bioluminescence was acquired with the IVIS system (Perkin Elmer, USA) and analyzed using the Living Image software (v4.2, Perkin Elmer). The clones presenting the highest expression (in terms of photons emitted per second) were selected, and named MM473: Luc and MM487: Luc. For *in vivo* studies, MM473: Luc and MM487: Luc were cultured in Ham's F-10 Nutrient Mixture medium, supplemented with 10% (v/v) FBS and 400 μg/mL of neomycin, and expanded in a 37 °C incubator with saturated humidity and 5% CO_2.

4.5. Cell cultures

NCI−H460, H460-R9A, A2780, A2780-Dx, NB4, U87-MG, HCT116, HT-29, U937, RAJI, REC-1, DG-75, U-2932, KM-H2, and L-428 cells were cultured in RPMI-1640 medium supplemented with 10% FBS, 2 mM L-glutamine and gentamicin sulfate. RAMOS, OCI-LY3, JECO-1, MAVER-2, MINO cells were cultured in RPMI-1640 medium supplemented with 20% FBS, 2 mM L-glutamine and gentamicin sulfate. Z-138 cells were cultured in IMDM medium supplemented with 10% FBS, L-glutamine and gentamicin sulfate. MDA-MB436 cells were cultured in DMEM medium supplemented with 10% FBS, 2 mM L-glutamine and gentamicin sulfate. MM473-Luc and MM487-Luc cells were cultured in Ham's F-10 Nutrient Mixture supplemented with 10% FBS, 2 mM L-glutamine, and G418 antibiotic. Cells were maintained in a 37 °C incubator with saturated humidity and an atmosphere of 95% air and 5% CO_2, and were sub-cultured every 2−3 days. Cells were monthly verified to be free of mycoplasma contamination.

The H460-R9A subline, resistant to ST1926, was generated as described in Zuco et al., 2005 [25]. The subline was maintained in the same culture conditions of the parental NCI−H460 cells.

4.6. Cell proliferation assay and flow cytometry

Cells in logarithmic phase of growth were seeded in 96-wells plastic plates, incubated overnight in culture medium, and exposed for 24 h to 10 scalar concentrations of the test compounds (8 replicates for each concentration). Upon a further 48 h growth in drug-free medium, cell survival was assessed by either sulphorhodamine B (SRB) (solid cancers) or tetrazolium-based (MTT) (hematological cancers) colorimetric assay and the IC_{50} value (drug concentration inhibiting 50% of cell growth) calculated by ALLFIT program.

The pro-apoptotic activity and the effect on cell cycle progression of the most active compounds was evaluated *in vitro* on various tumor cell lines by flow cytometry. To this end, cells were seeded in 10-cm tissue culture plates, allowed to attach, and incubated for 24 h, 48 h, and 72 h with the test compounds ($2 \times IC_{50}$ dose). After this, cells were harvested with trypsin/EDTA, rinsed with cold PBS, and fixed in 70% ice-cold ethanol at 4 °C. The day of analysis, cells were rinsed twice with cold PBS, incubated with RNase A (50 KU/ml) for 30 min at 37 °C, stained with propidium iodide (PI 50 μM) (Sigma Aldrich) and processed on a FACScan flow cytometer (Beckton Dickinson). The CellQuest software was used to acquire data, while cell cycle analysis was performed using the ModFit software. Histograms were generated by using FlowJo vX 10,0.7R2 (Tree Star., Inc, Ashland, OR).

4.7. HDACi assay

HDAC inhibition assay was performed by Reaction Biology Corp. (Malver, PA, USA). For the primary screening, ST1926, MIR002, and GEM144 were tested in a single dose (10 μM) against HDACs 1−11. HDAC reference compound Trichostatin A (TSA) and TMP269 were tested in a 10-dose IC_{50} with 3-fold serial dilution starting at 10 μM. Fluorogenic peptide 382 RHKK(Ac)AMC was used as fluorogenic substrate for HDAC 1,2,3,6,10. Fluorogenic HDAC Class 2a substrate (Trifluoroacetyl Lysine) was used for HDAC 4,5,7,9, and 11; Fluorogenic peptide RHK(Ac)K(Ac)AMC was used as substrate for HDAC 8.

For the evaluation of the IC_{50}, the compounds were tested in duplicate in 10-dose IC_{50} mode with 3-fold serial dilution starting at 10 μM against HDAC 11. HDAC reference compound Trichostatin A (TSA) was tested in a 10-dose IC_{50} with 3-fold serial dilution starting at 10 μM. IC_{50} values were calculated using the GraphPad Prism 4 program based on a sigmoidal dose-response equation. The blank (DMSO) value was entered as 1.00E-12 of concentration for curve fitting.

4.8. Primer extension assay

To determine direct POLA1 inhibition, an *in vitro* primer extension assay was performed as described in the paper from Han and colleagues with minor modifications [8]. Briefly, the primer extension substrate was generated by mixing 100 μL of a 5 M fluorescein labelled 15 nt RNA oligo (5-Fluorescein-rGrGrArAr-ArGrGrArCrGrArArArCrA-3), 100 μl of a 7.5 M 25 nt DNA oligo (5-(A) 6CCGGTGTTTCGTCCTTTCC-3), and 100 μL of 10 × reaction buffer (200 mM Tris-HCl, pH7.8, 100 mM $MgCl_2$, 20 mM DTT, and 500 mM NaCl). The mixture was heated to 75 °C for 2 min and gradually cooled to room temperature. Serial dilutions of ST1926, CD437, MIR002 and GEM144 were first prepared in DMSO, and then diluted in H_2O. The final concentrations used were 1.9 μM, 5.6 μM, 10 μM, 50 μM. One microliter of diluted compounds was added to 1U of POLA1 recombinant protein (Creative Biomart), 2 μL of 10 mg/mL BSA, and 0.4 μL of 2.5 mM dNTP and pre-incubated at 25 °C for 15 min. Afterwards, 3 μL of the primer extension substrate were added to the mixture. The primer extension reaction was incubated at 25 °C for 15 min, and then terminated via addition of 1 volume of 2X TBE-UREA sample buffer (Life Technologies). The reaction products were boiled for 2 min at 90 °C, resolved on a 15% TBE UREA gel and visualized using the Fluorescein acquisition program on the ChemiDoc XRS (Biorad).

4.9. Western blot analysis

For western blot, cells were lysed in RIPA buffer (50 mM Tris-HCl, pH 7.5, 150 mM NaCl, 1 mM EDTA, 1% NP40, 0.5% sodium dexoycholate, 0.1% sodium dodecyl sulfate, 1.5 mM Na_3VO_4, 10 mM sodium fluoride, 10 mM sodium pyrophosphate, 10 mM β-glycerolphosphate and EDTA-free protease inhibitor cocktail, Sigma Aldrich). Lysates were cleared by centrifugation at 13000 r.p.m. for 30 min at 4 °C. Laemmli Loading buffer (Biorad) was then added to a 1X final concentration and samples were separated by 4–20% SDS–PAGE gels (Biorad) and transferred to nitrocellulose membrane (BioRad). Membranes were blocked in TBS with 5% non-fat milk and 0.1% Tween20, and probed with primary antibodies overnight at 4 °C. Appropriate secondary antibodies HRP-conjugated were purchased from GE Healthcare (GENA934 and GENA931) and incubated for 1 h at room temperature. Chemioluminescence detection was done with the ECL HRP- substrate (RPN2232 GE Healthcare) and images were acquired on ChemiDoc XRS (Biorad).

Primary antibodies used were: Anti-Phospho Histone H2A.X (Millipore, 05–636); H2AX (abcam, ab11175) (p21 Waf1/Cip1, (CST #2947), Acetyl-p53 (Lys382) (CST, #2525), Total p53 (Santa Cruz, sc-393031), Histone H4 (CST, #2835), Anti-Acetyl Histone H4 (Millipore, 06598), PIN1 (Abcam, ab155283), p-ERK1/2 (Cell Signaling, #4370), ERK1/2 (CST, #4696), β-actin (Sigma, A5316), α-tubulin (Sigma, T5168), Anti-Acetylated alpha-Tubulin (abcam. ab24610), POLA1 (Elabscience, E-AB-31213), and GAPDH (CST, #2118).

4.10. qRT-PCR and ELISA

POLA1 expression in NCI–H4609 and H460-R9A cells was evaluated by qRT-PCR. Total RNA was extracted using Trizol (Invitrogen) according to manufacturer's instructions. One μg of RNA was then retrotranscribed by using the QuantiTech reverse transcripition Kit (QIAGEN 2050313), according to manufacturers' instruction. Quantitative real-time RT-PCR was performed on 10 ng of cDNA using the Power SYBR Green Master Mix (Thermo Fisher, 4367659) (Invitrogen) and the QuantStudio 7 thermocycler (Applied Biosystem). Primers employed for qRT-PCR analysis were: POLA1-FW 5′-GCTATGTGGAAGATGGCCGA-3′, POLA1-RV 5′-TGTTCGGTTTTGTCACTGCG-3′, and GAPDH-FW 5′-CCCCACCA-CACTGA ATCTCC-3′, GAPDH-RV 5′-TCTGCCCCAGACCCTAGAAT-3′. Experiments were performed in triplicates, and data were normalized to the housekeeping gene GAPDH. The relative abundance of transcripts was calculated by the comparative ΔΔCt method.

Evaluation of circulating IFN alpha proteins was measured by a commercially available ELISA Kit (ElabSCience, E-EL-M3054) according to the manufacturer's instructions. Serum samples from mice treated with vehicle or with MIR002 (N = 5 mice/group) were employed. GraphPad Prism® 6 software was used for interpolation with the standard curve.

4.11. Cytotoxicity and combination assays

The anti-proliferative effect of ST1926 was assessed, alone and in combination with SIS17 (Raybiotech, Inc; Cat # 332-12825-1; Lot # 140269RAY8), on human NCI–H460 and H460-R9A NSCLC cell lines. To do this, the cytotoxic activity of each single compound was first calculated. Indeed, predetermined numbers of cells in logarithmic phase of growth were seeded in 96-wells plastic plates, allowed to attach, and exposed for 72 h to 10 scalar concentrations of the test compounds (2-fold serial dilution series in culture medium). ST1926 was tested starting from 10 μM on NCI–H460 cells and from 50 μM on H460-R9A cells, while SIS17 from 100 μM on both cell lines. Cell survival was assayed by MTT test and the IC_{50} value (drug concentration inhibiting 50% of cell growth) calculated by ALLFIT program. For the combination studies, cells were seeded in 96-well plastic plates, allowed to attach, and exposed for 72 h to 5 sub-toxic, equipotent concentrations of the single drugs (4 replicates/dose) and their combinations (8 replicates/dose, 2-fold dilution series in culture medium, starting from nearby the IC50 value). ST1926 was tested starting 12 μM on H460-R9A cells, while SIS17 from 60 μM on both cell lines. Cell survival was assayed with the MTT test and the type of drugs interaction (synergism, antagonism, additivity) on cell growth was finally determined by assessing the Combination Index (CI) values with the CalcuSyn computer program.

4.12. In vivo experiments

MIR002 and GEM144 were dissolved to a concentration of 3.3 mg/mL in 10% DMSO, 5% ethanol, 20% Kolliphor® EL, and 65% Na_2CO_3 10 mM pH 11 and administered by gavage; ST1926 was dissolved to a concentration of 2 mg/mL in10% ethanol, 20% Kolliphor® EL, 70% saline solution and administered by gavage; cisplatin was dissolved to a concentration of 0.8 mg/mL in sterile saline solution and administered intravenously.

4–6 weeks old female CD-1 nude mice [Crl:CD1-Foxn1nu] (Charles River, FR or IT), were housed in individually ventilated cages on a 12 h light:12 h dark cycle at 20–24 °C and 45–65% humidity. Mice were allowed free access to sterilized diet and water. All experiments were in accordance with the European guidelines for the care and use of laboratory animals (2010/63/EU directive). The protocols were approved by the Biogem Ethics Committee and approved by the Italian Ministry of Health.

4.13. Xenograft models

4.13.1. Melanoma B16

1 × 105 mouse melanoma cells B16–F10-luc-G5 were resuspended in 200 μL M199 medium and inoculated subcutaneously in the right flank of ten C57BL/6 mice (Charles River). After 10 days from tumor implant (average tumor volumes were 320 mm^3), mice were divided in two groups and treated with MIR002 (5 mice, 50 mg/kg, twice a day for 5 days) or vehicle (5 mice). Five hours after the last administration, plasma was collected and analyzed by ELISA kit for the interferon alpha detection.

4.13.2. NCI H460 and H460-R9A

5 × 106H460 and H460-R9A, viable cells were resuspended in 200 μL M199 medium and subcutaneously inoculated on the right flank of each mouse (8 mice groups). Four days after inoculation, tumor masses were measured in length and width using a Mitutoyo caliper, mice were sorted basing on tumor volume (TV) and treatments were started following the schedules: MIR002 (p.o, Bid, 50 mg/kg; qd × 5 × 3 or 4 weeks); ST1926 (p.o.; 20 mg/kg; qd × 5 × 3 or 4 weeks); cisplatin (i.v.; 5 mg/kg; q7d × 4w). Tumor volume was calculated as follows: TV (mm3) = (Length (mm)x Width (mm)2). Tumor growth was followed by biweekly measurements. Tumor Growth Inhibition (TGI) for each group was calculated as follows: TGI (%) = 100 - (mean TVtreated/mean TVcontrol × 100).

4.13.3. MM473-luc and MM487-Luc

Cell lines (1 × 10^6) were re-suspended at concentration of in M199 medium. Tumor growth was monitored weekly with live imaging of bioluminescence using the IVIS technology (PerkinElmer). When bioluminescence values indicated stability of tumor growth in two consecutive measurements (usually 10–15 days from cells injection for MM473 and 21–28 days for MM487), mice were allocated in experimental groups. The treatments with MIR002 and GEM144 were performed orally (p.o) by using the schedules: Bid, 50 mg/kg; qd × 5 × 3 or 4 weeks); cisplatin was administered intravenously (i.v.) 5 mg/kg following the schedule q7d × 4w.

Tumor growth was evaluated weekly by using the IVIS Spectrum (PerkinElmer) *in vivo* technology system, through intraperitoneal injection of D-Luciferin potassium salt (100 μL/10 gr, PerkinElmer). After the IP D-luciferin injection, mice were anesthetized in an oxygen-rich induction chamber with 2% isofluorane, and images were captured 30 min after D-Luciferin injection to allow substrate distribution. Tumor volume was measured as average radiance that is the total flux of photons or radiance (photons/second from the surface) in each pixel, summed or integrated over the ROI area, in a square centimeter (cm^2) of the tissue. (photons/sec/cm^2/sr). The established maximum average radiance was 1×10^8 photons/sec/cm^2/sr, used as a humane end-point.

4.14. Statistical analysis

Tumor growth and body weight were measured every week. Statistical analyses were performed using non-parametric Mann-Whitney *U* Test and GraphPad Prism® 6 software.

4.15. Molecular modelling studies

Concerning the POLA1 enzyme, the simulations were performed by following the same procedure already described [19]. Briefly, docking calculations were carried out on the POLA1 structure co-crystallized with Aphidicolin and DNA-RNA duplex (PDB Id: 4Q5V) by using the GOLD program [7]. The searches were focused on a 10 Å radius sphere around the bound Aphidicolin and 100 poses were generated and ranked by the ChemPLP score for each ligand [54]. The so computed best poses were finally minimized using Amber [55].

The simulations on HDAC1 were based on the resolved HDAC1 structure in complex with a peptidomimetic inhibitor (H4K16Hx, PDV Id: 5ICN) [56]. This HDAC1 structure was chosen as the bound inhibitor comprises the same zinc binding group of the here proposed inhibitors (hydroxamic acid) and shows a remarkable molecular size which should assure a reasonably large binding cavity at least around the cavity rim. The protein structure was prepared by using the H++ tool which defines the ionization state of ionizable residues and selects both the histidine tautomers and the Asn/Gln arrangements [57]. The so completed structure was minimized by applying energy constraints to the metal ions and coordinating residues to retain them in the same geometry as seen in the resolved structure. Docking simulations were performed by using GOLD, focusing the search within a 10 Å radius sphere around the zinc ion and defining the possible geometries of the zinc chelation (i.e. tetrahedral or trigonal bipyramid). For each ligand, 100 poses were generated and ranked by the ChemPLP score. The reliability of these settings was assessed by a re-docking simulation of the H4K16Hx ligand. The obtained pose was able to reproduce the correct arrangement of the ZBG group while a certain degree of discrepancy was observed in the arrangement of the cap moieties which was acceptable when considering both the flexibility of this peptidomimetic ligand and the crystal resolution (3.3 Å).

Since no resolved HDAC11 structure was available, a homology model was generated by considering that HDAC11 is the only member of class IV which is phylogenetically close to class I. Hence, the HDAC11 primary sequence (Uniprot Id: Q96DB2) was compared with those of class I (i.e. with HDAC1: Q13547, HDAC2: Q92769, HDAC3: O15379, HDAC8: Q9BY41) by multiple alignment using Clustal W (using BLOSUM matrix with Gap Opening Penalty = 10.0 and Gap Extension Penalty = 0.05) [58]. Such a multiple alignment reveals that HDAC8 should be the optimal template with a sequence identity = 26.86% and E-value BLAST = 5 E−18. Hence, the chosen resolved HDAC8 structure was that in complex with quisinistat (an hydroxamic acid-based inhibitor, PDB Id: 5HSK) [59]. In detail, 10 homology models were generated by Modeller9.23 using the cited template and the above described multiple alignment [60]. The best obtained model shows satisfactory characteristics as confirmed by the computed scores (DOPE = −33007.71 and GA341 = 1) and the percentage of residues falling within the allowed regions of the Ramachandran plot = 87.58%. By superimposing the homology model with the resolved template, the pose of Zn^{++} and K^+ ions were defined as well as that of the water which coordinates the K^+ ion. The model was then completed by using the H++ software as described above and underwent energy minimization using Amber as described for HDAC1. Docking simulations were performed by GOLD applying the same settings already adopted for HDAC1 and the best computed complexes were minimized by using Amber.

Declaration of competing interest

The authors declare that they have no known competing financial interests or personal relationships that could have appeared to influence the work reported in this paper.

Acknowledgements

The authors gratefully acknowledge Prof. Lucio Merlini for helpful suggestions and discussion.

Appendix A. Supplementary data

Supplementary data to this article can be found online at https://doi.org/10.1016/j.ejmech.2021.113971.

References

[1] R. Sundar, N. Valeri, K.J. Harrington, T.A. Yap, Combining molecularly targeted agents: is more always better? Clin. Cancer Res. 23 (2017) https://doi.org/10.1158/1078-0432.CCR-16-2399.
[2] T. Stanković, J. Dinić, A. Podolski-Renić, L. Musso, S.S. Burić, S. Dallavalle, M. Pešić, Dual inhibitors as a new challenge for cancer multidrug resistance treatment, Curr. Med. Chem. 26 (2019) 6074–6106, https://doi.org/10.2174/0929867325666180607094856.
[3] S. Dallavalle, V. Dobričić, L. Lazzarato, E. Gazzano, M. Machuqueiro, I. Pajeva I. Tsakovskag, N. Zidarh, R. Fruttero, Improvement of conventional anti-cancer drugs as new tools against multidrug resistant tumors, Drug Resist. Updates 50 (2020), 100682, https://doi.org/10.1016/j.drup.2020.100682.
[4] S.-Y. Seo, Multi-targeted hybrids based on HDAC inhibitors for anti-cancer drug discovery, Arch Pharm. Res. (Seoul) 35 (2012) 197–200, https://doi.org/10.1007/s12272-012-0221-9.
[5] P.M.J. Burgers, T.A. Kunkel, Eukaryotic DNA replication fork, Annu. Rev. Biochem. 86 (2017) 417–438, https://doi.org/10.1146/annurev-biochem-061516-044709.
[6] P. Starokadomskyy, T. Gemelli, J.J. Rios, C. Xing, R.C.H. Li, V. Pokatayev, I. Dozmorov, S. Khan, N. Miyata, G. Fraile, P. Raj, Z. Xu, Z. Xu, L. Ma, Z. Lin, H. Wang, Y. Yang, D. Ben-Amitai, N. Orenstein, H. Mussaffi, E. Baselga, G. Tadini, E. Grunebaum, Adrijan Sarajlija, K. Krzewski, E.K. Wakeland, N. Yan, M.T. de la Morena, A.R. Zinn, E. Burstein, DNA polymerase-α regulates the activation of type I interferons through cytosolic RNA: DNA synthesis, Nat. Immunol. 17 (2016) 495–504, https://doi.org/10.1038/ni.3409.
[7] A.G. Baranovskiy, N.D. Babayeva, Y. Suwa, Y.I. Pavlov, T.H. Tahirov, Structural basis for inhibition of DNA replication by aphidicolin, Nucleic Acids Res. 42 (2014) 14013–14021, https://doi.org/10.1093/nar/gku1209.
[8] L. Sun, L. Chen, H. Li, Checkpoint-modulating immunotherapies in tumor treatment: targets, drugs, and mechanisms, Int. Immunopharm. 67 (2019) 160–175, https://doi.org/10.1016/j.intimp.2018.12.006.
[9] T. Han, M. Goralski, E. Capota, S.B. Padrick, J. Kim, Y. Xie, D. Nijhawan, The anti-tumor toxin CD437 is a direct inhibitor of DNA Polymerase α, Nat. Chem. Biol.

7 (2016) 511−515, https://doi.org/10.1038/nchembio.2082.
[10] P. Dollé, K. Niederreither (Eds.), The Retinoids, Biology, Biochemistry and Disease Wiley, New York, 2015.
[11] R.G. Keedwell, Y. Zhao, L.A. Hammond, S. Qin, K.-Y. Tsang, A. Reitmair, Y. Molina, Y. Okawa, L.I. Atangan, D. Lee Shurland, K. Wen, D.M.A. Wallace, R. Bird, R.A.S. Chandraratna G. Brown, A Retinoid-related molecule that does not bind to classical retinoid receptors potently induces apoptosis in human prostate cancer cells through rapid caspase activation, Cancer Res. 64 (2004) 3302−3312, https://doi.org/10.1158/0008-5472.CAN-03-2763.
[12] F.J. Piedrafita, M.A. Ortiz, Mechanism of action and therapeutic potential of novel adamantyl retinoid-related molecules, Curr. Cancer Ther. Rev. 2 (2006) 185−198, https://doi.org/10.2174/157339406776872852.
[13] E. Parrella, M. Giannì, M. Fratelli, M.M. Barzago, I. Raska Jr., L. Diomede, M. Kurosaki, C. Pisano, P. Carminati, L. Merlini, S. Dallavalle, M. Tavecchio, C. Rochette-Egly, M. Terao, E. Garattini, Antitumor activity of the retinoid-related molecules (E)-3-(4′-Hydroxy-3′-adamantylbiphenyl-4-yl)acrylic acid (ST1926) and 6-[3-(1-Adamantyl)-4-hydroxyphenyl]-2-naphthalene carboxylic acid (CD437) in F9 teratocarcinoma: role of retinoic acid receptor γ and retinoid-independent pathways, Mol. Pharmacol. 70 (2006) 909−924, https://doi.org/10.1124/mol.106.023614.
[14] R. Cincinelli, S. Dallavalle, L. Merlini, S. Penco, C. Pisano, P. Carminati, V. Zuco, C. Zanchi, F. Zunino, Synthesis and structure−activity relationships of a new series of retinoid-related biphenyl-4-ylacrylic acids endowed with antiproliferative and proapoptotic activity, J. Med. Chem. 48 (2005) 4931−4946, https://doi.org/10.1021/jm049440h.
[15] P. Aouad, M. Saikali, R. Abdel-Samad, S. Fostok, L. El-Houjeiri, C. Pisano R. Talhouk, N. Darwiche, Antitumor activities of the synthetic retinoid ST1926 in two-dimensional and three-dimensional human breast cancer models, Anti Cancer Drugs 28 (2017) 757−770, https://doi.org/10.1097/CAD.0000000000000511.
[16] R.R. Nasr, R.A. Hmadi, R.M. El-Eit, A.N. Iskandarani, M.N. Jabbour, G. Zaatari G, F.-X. Mahon, C. Pisano, N. Darwiche, ST1926, an orally active synthetic retinoid, induces apoptosis in chronic myeloid leukemia cells and prolongs survival in a murine model, Int. J. Cancer 137 (2015) 698−709, https://doi.org/10.1002/ijc.29407.
[17] H. Basma, S.E. Ghayad, G. Rammal, A. Mancinelli, M. Harajly, F. Ghamloush, L. Dweik, R. El-Eit, H. Zalzali, W. Rabeh, C. Pisano, N. Darwiche, R. Saab, The synthetic retinoid ST1926 as a novel therapeutic agent in rhabdomyosarcoma, Int. J. Cancer 138 (2016) 1528−1537, https://doi.org/10.1002/ijc.29886.
[18] R. Abdel-Samad, P. Aouad, H. Gali-Muhtasib, Z. Sweidan, R. Hmadi, H. Kadara, E.L. D'Andrea, A. Fucci, C. Pisano, N. Darwiche, Mechanism of action of the atypical retinoid ST1926 in colorectal cancer: DNA damage and DNA polymerase α, Am J Cancer Res 8 (2018) 39−55.
[19] R. Cincinelli, L. Musso, M.B. Guglielmi, I. La Porta, A. Fucci, E.L. D'Andrea, F. Cardile, F. Colelli, G. Signorino, N. Darwiche, S. Gervasoni, G. Vistoli, C. Pisano, S. Dallavalle, Novel adamantyl retinoid-related molecules with POLA1 inhibitory activity, Bioorg. Chem. 104 (2020), 1042532, https://doi.org/10.1016/j.bioorg.2020.104253.
[20] N. Darwiche, Epigenetic mechanisms and the hallmarks of cancer: an intimate affair, Am J Cancer Res 10 (2020) 1954−1978.
[21] M. Manal, M.J. Chandrasekar, J. Gomathi Priya, M.J. Nanjan, Inhibitors of histone deacetylase as antitumor agents: a critical review, Bioorg. Chem. 67 (2016) 18−42, https://doi.org/10.1016/j.bioorg.2016.05.005.
[22] J. Roche, P. Bertrand, Inside HDACs with more selective HDAC inhibitors, Eur. J. Med. Chem. 121 (2016) 451−483, https://doi.org/10.1016/j.ejmech.2016.05.047.
[23] Q. Zhang, X. Cao, Epigenetic regulation of the innate immune response to infection, Nat. Rev. Immunol. 19 (2019) 417−432, https://doi.org/10.1038/s41577-019-0151-6.
[24] F. Sala, M. Zucchetti, R. Bagnati, M. D'Incalci, S. Pace, F. Capocasa, E. Marangon, Development and validation of a liquid chromatography−tandem mass spectrometry method for the determination of ST1926, a novel oral antitumor agent, adamantyl retinoid derivative, in plasma of patients in a Phase I study, J. Chromatogr. B Analyt. Technol. Biomed. Life Sci. 877 (2009) 3118−3126, https://doi.org/10.1016/j.jchromb.2009.08.001.
[25] V. Zuco, C. Zanchi, C. Lanzi, G.L. Beretta, R. Supino, C. Pisano, M. Barbarino, R. Zanier, F. Bucci, C. Aulicino, P. Carminati, F. Zunino, Development of resistance to the atypical retinoid, ST1926, in the lung carcinoma cell line H460 is associated with reduced formation of DNA strand breaks and a defective DNA damage response, Neoplasia 7 (2005) 667−677, https://doi.org/10.1593/neo.05127.
[26] J.E. Bradner, N. West, M.L. Grachan, E.F. Greenberg, S.J. Haggarty, T. Warnow, R. Mazitschek, Chemical phylogenetics of histone deacetylases, Nat. Chem. Biol. 6 (2010) 238−243, https://doi.org/10.1038/nchembio.313.
[27] S.S. Liu, F. Wu, Y.M. Jin, W.Q. Chang, T.M. Xu, HDAC11: a rising star in epigenetics, Biomed. Pharmacother. 131 (2020) 110607, https://doi.org/10.1016/j.biopha.2020.110607.
[28] C. Yanginlar, C. Logie, HDAC11 is a regulator of diverse immune functions, BBA-Gene Regulatory Mechanisms 1861 (2018) 54−59, https://doi.org/10.1016/j.bbagrm.2017.12.002.
[29] N. Bora-Singhal, D. Mohankumar, B. Saha, C.M. Colin, J.Y. Lee, M.W. Martin, X. Zheng, D. Coppola S. Chellappan, Novel HDAC11 inhibitors suppress lung adenocarcinoma stem cell self-renewal and overcome drug resistance by suppressing Sox2, Sci. Rep. 10 (2020), 4722, https://doi.org/10.1038/s41598-020-61295-6.
[30] M.W. Martin, J.Y. Lee, D.R. Lancia, P.Y. Ng, B. Hana, J.R. Thomason, M.S. Lynes, C.G. Marshall, C. Conti, A. Collis, M. Alvarez Morales, K. Doshi, A. Rudnitskaya, L. Yao, X. Zheng, Discovery of novel N-hydroxy-2-arylisoindoline-4-carboxamides as potent and selective inhibitors of HDAC11, Bioorg. Med. Chem. Lett 28 (2018) 2143−2147, https://doi.org/10.1016/j.bmcl.2018.05.021.
[31] S.I. Son, J. Cao, C.-L. Zhu, S.P. Miller, H. Lin, Activity-guided design of HDAC11-specific inhibitors, ACS Chem. Biol. 14 (2019) 1393−1397, https://doi.org/10.1021/acschembio.9b00292.
[32] C. Maffeo, H.Y. Chou, A. Aksimentiev, Molecular mechanisms of DNA replication and repair machinery: insights from microscopic simulations, Adv Theory Simul 2 (2019), 1800191, https://doi.org/10.1002/adts.201800191.
[33] K.V. Butler, J. Kalin, C. Brochier, G. Vistoli, B. Langley, A.P. Kozikowski, Rational design and simple chemistry yield a superior, neuroprotective HDAC6 inhibitor, tubastatin A, J. Am. Chem. Soc. 132 (2010) 10842−10846, https://doi.org/10.1021/ja102758v.
[34] C.-Y. Gui, L. Ngo, W.S. Xu, V.M. Richon, P.A. Marks, Histone deacetylase (HDAC) inhibitor activation of p21WAF1 involves changes in promoter-associated proteins, including HDAC1, Proc. Natl. Acad. Sci. Unit. States Am. 101 (2004) 1241−1246, https://doi.org/10.1073/pnas.0307708100.
[35] P. Chun, Histone deacetylase inhibitors in hematological malignancies and solid tumors, Arch Pharm. Res. (Seoul) 38 (2015) 933−949, https://doi.org/10.1007/s12272-015-0571-1.
[36] S.-H. Min, X.Z. Zhou, K.P. Lu, The role of Pin1 in the development and treatment of cancer *Arch*, Pharm. Res. (N. Y.) 39 (2016) 1609−1620.
[37] T. Khatib, P. Marini, S. Nunna, D.R. Chisholm, A. Whiting, C. Redfern, I.R. Greig, P. McCaffery, Genomic and non-genomic pathways are both crucial for peak induction of neurite outgrowth by retinoids Cell, Commun signal 17 (2019) 40.
[38] W. Wang, L. Fu, S. Li, Z. Xu, X. Li, Histone deacetylase 11 suppresses p53 expression in pituitary tumor cells, Cell Biol. Int. 41 (2017) 1290−1295, https://doi.org/10.1002/cbin.10834.
[39] D. Gong, Z. Zeng, F. Yi, J. Wu, Inhibition of histone deacetylase 11 promotes human liver cancer cell apoptosis, Am J Transl Res 11 (2019) 983−990.
[40] A. Ercilla, J. Benada, S. Amitash, G. Zonderland, G. Baldi, K. Somyajit K, F. Ochs, V. Costanzo, J. Lukas, L. Toledo, Physiological tolerance to ssDNA enables strand uncoupling during DNA replication, Cell Rep. 30 (2020) 2416−2429, https://doi.org/10.1016/j.celrep.2020.01.067.
[41] D.A. Nalawansha, I.D. Gomes, M.K. Wambua, M. Kay, H. Pflum, HDAC inhibitor-induced mitotic arrest is mediated by Eg5/KIF11 acetylation, Cell Chemical Biology 24 (2017) 481−492, https://doi.org/10.1016/j.chembiol.2017.03.008.
[42] Y. Nunez-Alvarez, M. Suelves, HDAC11: a multifaceted histone deacetylase with proficient fatty deacylase activity and its roles in physiological processes, FEBS J. (2021), https://doi.org/10.1111/febs.15895.
[43] H.E. Deubzer, M.C. Schier, I. Oehme, M. Lodrini, B. Haendler, A. Sommer, O. Witt, HDAC11 is a novel drug target in carcinomas, Int. J. Cancer 132 (2013) 2200−2208, https://doi.org/10.1002/ijc.27876.
[44] J. Cao, L. Sun, P. Aramsangtienchai, N.A. Spiegelman, X. Zhang, W. Huang, E. Seto, H. Lin, HDAC11 regulates type I interferon signaling through defatty-acylation of SHMT2, Proc. Natl. Acad. Sci. Unit. States Am. 116 (2019) 5487−5492, https://doi.org/10.1073/pnas.1815365116.
[45] C. Yanginlar, C. Logie, HDAC11 is a regulator of diverse immune functions, Biochim Biophys Acta Gene Regul Mech 1861 (2018) 54−59, https://doi.org/10.1016/j.bbagrm.2017.12.002.
[46] A. Ortiz, S.Y. Fuchs, Anti-metastatic functions of type 1 interferons: foundation for the adjuvant therapy of cancer, Cytokine 89 (2017) 4−11, https://doi.org/10.1016/j.cyto.2016.01.010.
[47] H.M. Lazear, J.W. Schoggins, M.S. Diamond, Shared and distinct functions of type I and type III interferons, Immunity 50 (2019) 907−923, https://doi.org/10.1016/j.immuni.2019.03.025.
[48] S. Booy, L. Hofland, C. van Eijck, Potentials of interferon therapy in the treatment of pancreatic cancer, J. Interferon Cytokine Res. 35 (2015) 327−339, https://doi.org/10.1089/jir.2014.0157.
[49] R. Di Troli, E. Simeone, G. Di Lorenzo, C. Buonerba, P.A. Ascierto, The use of interferon in melanoma patients: a systematic review, Cytokine Growth Factor Rev. 26 (2015) 203−212, https://doi.org/10.1016/j.cytogfr.2014.11.008.
[50] E.C. Borden, Interferons α and β in cancer: therapeutic opportunities from new insights, Nat. Rev. Drug Discov. 18 (2019) 219−234, https://doi.org/10.1038/s41573-018-0011-2.
[51] Y. Yoshikawa, K. Kuribayashi, T. Minami, M. Ohmuraya, T. Kijima, Epigenetic alterations and biomarkers for immune checkpoint inhibitors-current standards and future perspectives in malignan pleural mesothelioma treatment, Front Oncol 10 (2020), 554570, https://doi.org/10.3389/fonc.2020.554570.
[52] G. Giannini, T. Brunetti, G. Battistuzzi, D. Alloatti, G. Quattrociocchi, M.G. Cima, L. Merlini, S. Dallavalle, R. Cincinelli, R. Nannei, L. Vesci, F. Bucci, R. Foderà, M.B. Guglielmi, C. Pisano, W. Cabri, New retinoid derivatives as back-ups of Adarotene, Bioorg. Med. Chem. 20 (2012) 2405−2415, https://doi.org/10.1016/j.bmc.2012.01.042.
[53] R. Vázquez, S.A. Licandro, L. Astorgues-Xerri, E. Lettera, N. Panini, M. Romano, E. Erba, P. Ubezio, E. Bello, R. Libener, S. Orecchia, F. Grosso, M.E. Riveiro, E. Cvitkovic, M. Bekradda, M. D'Incalci, R. Frapolli, Promising in vivo efficacy of the BET bromodomain inhibitor OTX015/MK-8628 in malignant pleural mesothelioma xenografts, Int. J. Cancer 140 (2017) 197−207, https://doi.org/10.1002/ijc.30412.
[54] G. Jones, P. Willett, R.C. Glen, A.R. Leach, R. Taylor, Development and

validation of a genetic algorithm for flexible docking, J. Mol. Biol. 267 (1997) 727–748, https://doi.org/10.1006/jmbi.1996.0897.
[55] J. Wang, W. Wang, P.A. Kollman, D.A. Case, Automatic atom type and bond type perception in molecular mechanical calculations, J. Mol. Graph. Model. 25 (2006) 247–260, https://doi.org/10.1016/j.jmgm.2005.12.005.
[56] P.J. Watson, C.J. Millard, A.M. Riley, N.S. Robertson, L.C. Wright, H.Y. Godage, S.M. Cowley, A.G. Jamieson, B.V.L. Potter, J.W.R. Schwabe, Insights into the activation mechanism of class I HDAC complexes by inositol phosphates, Nat. Commun. 7 (2016), 11262, https://doi.org/10.1038/ncomms11262.
[57] J.C. Gordon, J.B. Myers, T. Folta, V. Shoja, L.S. Heath, A. Onufriev, H++: a server for estimating pKas and adding missing hydrogens to macromolecules, Nucleic Acids Res. 33 (2005) W368–W371.
[58] J.D. Thompson, D.G. Higgins, T.J. Gibson, W. Clustal, Improving the sensitivity of progressive multiple sequence alignment through sequence weighting, position-specific gap penalties and weight matrix choice, Nucleic Acids Res. 22 (1994) 4673–4680.
[59] M. Sippl, W, C. Romier, Characterization of histone deacetylase 8 (HDAC8) selective inhibition reveals specific active site structural and functional determinants, J. Med. Chem. 61 (2018) 10000–10016.
[60] B. Webb, A. Sali, Protein structure modeling with MODELLER, Methods Mol. Biol. 1654 (2017) 39–54.